Title
Mechanisms and Regulation of Cellulose Degradation by Fungal Enzymes

Author
Gunda, Padma Rekha

Publication Date
2011

Peer reviewed|Thesis/dissertation

Mechanisms and Regulation of Cellulose Degradation by Fungal Enzymes

by

Padma Rekha Gunda

A dissertation submitted in partial satisfaction of the

requirements for the degree of

Doctor of Philosophy

in

Molecular and Cell Biology

in the

Graduate Division

of the

University of California, Berkeley

Committee in charge:

Professor Jamie Cate, Chair

Professor Michael Marletta

Professor Richard Calendar

Professor Chris Somerville

Fall 2011

Abstract

Mechanisms and Regulation of Cellulose Degradation by Fungal Enzymes

by

Padma Rehka Gunda

Doctor of Philosophy in Molecular and Cell Biology

University of California, Berkeley

Professor Jamie Cate, Chair

Liquid fuels derived from plant biomass have the potential to contribute to sustainability efforts. However, the conversion of plant biomass is very difficult due to its complex nature. Cellulose, the primary component of plant cell walls, is a recalcitrant polysaccharide comprised of glucose. In nature, various fungi and bacteria enzymatically depolymerize cellulose for consumption. Understanding how cellulases are produced and function will be invaluable to the realization of cellulosic biofuels. The work here describes how a prominent cellulase interacts with cellulose during depolymerization, and how the cellulolytic fungus *Neurospora crassa* in part signals for the production of cellulase enzymes.

The interactions of cellulases with cellulose are not well understood due to the recalcitrance and heterogeneity of the solid substrate. Cellobiohydrolase I, the most prominent cellulase in many fungal systems, was fluorescently labeled and monitored on the surface of crystalline cellulose. Four classes of behaviors were observed for this enzyme on the surface of cellulose: productive and linear movement, nonproductive surface diffusion, stationary, and transient association. In parallel, changes to the surface of crystalline cellulose were observed with atomic force microscopy to characterize how this enzyme modifies its substrate after degradation.

The processes that initiate cellulase induction in *Neurospora crassa* have yet to be identified. A screen of deletion strains grown on cellulose was performed to isolate regulators of cellulase production. A kinase (NCU07399) was identified as a regulator of the transcriptional activation of several cellulase genes. Deletion of this kinase in *Neurospora* reduces the upregulation of cellulases by as much as 50-fold and also induces the secretion of a metalloprotease. The results here provide a basis for exploring the pathways involved in *N. crassa* cellulase production.

Table of Contents

List of Figures

List of Tables

To my sister and to my parents.

1. Introduction to Cellulose Degradation

1.1 Biofuels and Plant Cell Walls

Every year, terrestrial plants convert over 100 billion metric tons of CO_2 into cellulose [1]. Cellulose, the most abundant biomolecule on earth, serves to provide structural stability to the plant cell wall and is a polymer comprised of β(1→4) linked glucose units. In the plant cell wall, cellulose forms a complex matrix with other polysaccharides and lignin, a cross-linked aromatic polymer [2] [3]. The enzymatic degradation of plant cell walls by various organisms is a key step in nature that contributes to the global carbon cycle [4].

In the coming decades, a major challenge will be to transition our current fossil fuel-based economy to one that is more sustainable. Liquid fuels are currently the standard for the global transportation sector, and will likely continue to be due to our deep-rooted infrastructure. However, biofuels have the potential to displace the petroleum-based versions we now use, with very low carbon emissions. [5]

In the United States, current methods for ethanol production acquire fermentable sugars almost exclusively from grain-based feedstocks such as corn and wheat. Unfortunately, fuel from these sources contains only marginally more energy than that required to grow, harvest, and convert the starch into fuel, making the overall procedure far from economical or carbon-efficient [5]. Consequently, new efforts have been directed toward the enzymatic production of biofuels from cellulose [6].

Despite its simple chemical composition, cellulose is extremely recalcitrant to depolymerization, as its purpose is to provide stability to the plant cell wall [7]. Glycan chains (chains of glucose) hydrogen bond to each other to form a compact, crystalline solid impenetrable to enzymes and most chemical compounds. Cellulose can also display a great deal of polymer heterogeneity, making its degradation even more complicated. Moreover, matrix polysaccharides and lignin coat cellulose fibers in the plant cell wall and act as a physical barrier to it [8]. Thus the complete digestion of cellulose is an enzymatic challenge. Increasing the efficiency of cellulose degradation will be necessary for the industrial scale production of cellulosic biofuels [8-10].

Certain bacteria and fungi degrade plant cell walls for their consumption. If a greater understanding of how these organisms depolymerize cellulose is acquired, one could exploit those mechanisms for biofuel production [11]. Indeed, applying and improving mechanisms found in nature is an integral component of many approaches toward biomass-to-bioenergy conversion [12, 13].

1.2 Cellulases

Several types of bacteria and fungi use cellulose as their primary energy and carbon source [14, 15]. These organisms exist in a wide variety of environments to which each has adapted. Consequently, there is great diversity in cellulose-degrading enzyme (cellulase) systems found in fungi and bacteria, unsurprising given the nature of this substrate. Cellulose is a recalcitrant solid showing a great deal of polymer heterogeneity, and, as such, its hydrolysis is a surface science that does not follow standard kinetic models [16, 17]. Many different types of enzymes are needed to

operate at the liquid-solid interface to efficiently degrade this stable polysaccharide. Cellulases are classified by either their mode of action or into families by their sequence similarity. There are over 125 glycoside hydrolase (GH) families categorized by sequence similarity [18, 19], among which are five main cellulase functional classes.

Exoglucanases are hydrolytic enzymes that operate on a glycan chain end. They most often cleave two, three, or four glucose units at a time, releasing the cellodextrins (cellobiose, cellotriose, cellotetraose) into solution. They are also referred to as cellobiohydrolases, as their primary product is cellobiose, and most often from GH families 6, 7, 9, and 48. In most cellulase systems, exoglucanases are the most highly represented enzymes. Though usually only a couple of types exist in an organism, exoglucanases comprise the majority of cellulases produced [20]. These enzymes are the most capable of depolymerizing crystalline cellulose into soluble sugar due to their processivity along a glycan chain [21-22]. Tunnel-like active sites allow a chain to be thread through the enzyme, possibly preventing enzyme dissociation after each round of hydrolysis [23]. Exoglucanases also often contain Carbohydrate-Binding Modules (CBMs) for the attachment to cellulose, allowing them to remain bound on the surface of cellulose as they find the end of a glycan chain [24].

Endoglucanases operate at an internal site of the glycan chain. By doing so, they create new chain ends onto which exoglucanases can act. In a complementary manner, exoglucanases depolymerize a glycan chain on the surface and thereby expose new chains underneath. Thus a strong synergism exists between endo- and exocellulases—each creates new sites of attack for the other. Endoglucanases are commonly found in GH families 5, 9, 44, and 45. [25]

β-glucosidases do not act on cellulose, per se, but rather on the primary products of its depolymerization. These enzymes hydrolyze cellodextrins into glucose monomers. They are essential for alleviating the product inhibition of cellobiohydrolases during cellulose degradation [26]. Their action also enables the cell to uptake sugar in the form of glucose. There are also intracellular β-glucosidases in some organisms, which enable the uptake of sugar in the form of cellodextrins [77].

Most enzymes related to cellulose digestion involve the hydrolysis of linked sugars. However, there also exist non-hydrolytic enzymes essential for enhanced cellulose degradation. Oxidative enzymes, such as cellobiose dehydrogenase, interact with cellulose though redox reactions [27]. Lastly, cellulose phosphorylases depolymerize cellulose with phosphate instead of water [28].

1.3 *Neurospora crassa* as a model cellulase producer

Neurospora crassa is a cellulolytic, filamentous fungus that over the last 80 years has been widely used to study numerous eukaryotic processes, such as DNA repair and cellular differentiation [30, 31]. Additionally, it is an NIH model organism for many non-yeast fungal species, including various plant and animal pathogens, though it is not a pathogen itself [32]. As a model organism, there are a multitude of molecular and genetic techniques available.

In a 1941 *Neurospora crassa* study, Tatum and Beadle proposed the influential hypothesis that a single gene encodes for a single protein [33]. It was later learned that

N. crassa has mechanisms in place to maintain only one copy of any gene, and thereby prevent gene duplication [44]. In 2003, the *N. crassa* genome was sequenced [45]. As a result of these two occurrences, a near-complete gene knockout library has been made, creating strains with the deletion of almost any protein—further adding to the tools of this organism and making it an ideal system for new studies [46].

Trichoderma reesei is the most studied cellulolytic fungus, and has been modified to produce extremely high levels of cellulases, up to 100 g/L [41]. *T. reesei* has been characterized for over 60 years and is considered an industrial workhorse for cellulase enzymes. However, in 2008 its genome sequence was released and found to contain fewer cellulase genes than any other cellulolytic fungal genome previously sequenced [47]. This discovery was unexpected given the robust degradative capabilities of engineered strains, and suggested there was potential for other celluloytic fungi to both gain industrial relevance and outperform *T. reesei* [41].

Due to the many tools in *Neurospora crassa*, as well as the potential for the development of its cellulase system, our lab and collaborators conducted combined transcriptome/secretome analysis on *N. crassa* grown on cellulose [48]. Microarray data revealed the significant upregulation of approximately 200 genes after exposure to cellulose. This work shed light on a number of previously unknown components involved in processes surrounding the sensing, degradation, and consumption of cellulose. It has thus created a platform for much future work.

1.4 Research Objectives

Cellulose degradation involves many complex processes and being able to manipulate these would greatly aid the production of biofuels. Thus, a detailed understanding of cellulase production and mechanism is a major research goal. Cellobiohydrolases are the most prominent enzymes in cellulase systems but their interactions with cellulose are not well understood due to the heterogeneity and recalcitrance of the substrate. In the following pages, the behavior of *T. reesei* Cellobiohydrolase I on the surface of crystalline cellulose is described. This work was conducted with single molecule fluorescence microscopy to monitor fluorescently-labeled enzymes. Changes to the surface of crystalline cellulose were also monitored with atomic force microscopy to characterize how this enzyme modifies its substrate after degradation.

Neurospora crassa upregulates many genes, including cellulases, in the presence of cellulose. Yet the means by which the presence of cellulose is signaled to the nucleus remains unknown. In Chapter 3, work to investigate the cellulose signaling network of *N. crassa* is described. A screen of deletion strains was performed, examining to what extent various possible signaling enzymes contribute to *N. crassa*'s to degrade cellulose. One kinase deletion strain with very severe effects and its corresponding kinase were further characterized to identify the role of the kinase in signaling of cellulase induction.

2. Biophysical Studies of *T. Reesei* Cellobiohydrolase I on Crystalline Cellulose

This work was carried out in collaboration with Charlie Chen, Haw Yang, and Daniel Fletcher.

2.1 Cellulases at Liquid-Solid Interfaces

Crystalline cellulose is depolymerized by the synergistic action of endo- and exoglucanases. Endoglucanases locate sites along a glycan chain, possibly found at random, and insert a water molecule into the glycosidic β–(1,4) bond, creating two new chain ends on either side of the cleaved linkage. Glycan chains in cellulose have a directional polarity, and thus the new end created before the glycosidic bond cleavage exposes different chemical moieties than the sugar residue after the cleavage. The first end is referred to as the reducing end, due to the fact that an aldehyde with reducing capabilities is exposed. The other end is referred to as the nonreducing end. As previously mentioned, most organisms only contain a couple varieties of cellobiohydrolases [20]. Between these two exoglucanase types, generally one operates at the reducing end, while the other acts on the nonreducing end, to processively digest cellulose. Thus a synergism can exist between exoglucanases as well as with endoglucanases. Water molecules may occupy the space underneath the nonreducing end, thereby preventing its reannealing to the rest of the cellulose crystal [49]. This would aid an exoglucanase to extract and solvate a chain from the cellulose solid, and thread it through the enzyme's active site tunnel (Figure 2-1). The pulling of glycan chains from cellulose and their threading through enzymes (the complexation of cellulases and cellulose) is thought to be the rate-limiting step in cellulase action, not hydrolysis [50].

Cellulases and other glycosyl hydrolases contain catalytic aspartate or glutamate residues that hydrolyze cellulose through either acid-base assistance, or through acid-base chemistry plus nucleophilic attack. The first type results in a one-step concerted mechanism and an inversion of stereochemistry at the terminal hydroxyl. The second is a two-step, double-displacement mechanism involving a covalent glycosyl-enzyme intermediate before water addition. This Koshland-type mechanism leaves the terminal C1 hydroxyl in the β configuration, a retention of its original stereochemistry. [51,52]

Cellobiohydrolase I (CBH I) comprises approximately 60% of secreted *T. reesei* cellulases [54]. It contains a carbohydrate-binding module, which is connected to the catalytic domain through a flexible, glycosylated linker [49]. A 5nm-long tunnel runs through the catalytic domain (Figure 2-1), and this enzyme operates from the reducing end toward the nonreducing end [55]. Cellobiohydrolase I is considered a strict exoglucanase that shows little or no endo-activity [56]. It is also considered the most processive of all cellulases, meaning a bound enzyme will not likely dissociate from a glucan chain before its complete degradation [57].

Numerous studies have been performed to determine the level of processivity of CBH I [58-60]. Among these studies, there is no consensus for how long CBH I will digest a glucan chain before dissociation. Using different methods, each predicts a different processivity index, ranging from approximately five to 85 cleavages [58-60]. This corresponds to travelling approximately 5-85 nm linearly along a glucan chain

before either dissociation or inactivation. The assorted interactions of cellulases with their substrate before, during, and after hydrolysis are not well understood. As a surface science, certain aspects of cellulose breakdown have eluded characterization by conventional in-solution techniques and standard kinetic models. The following microscopy work explores the complex dynamics between enzyme and solid substrate. Single molecule fluorescence microscopy was used to track fluorescently labeled CBH I on the surface of crystalline cellulose. Atomic force microscopy was used to characterize the surface of cellulose before and after enzyme treatments.

2.2 Results and Discussion

2.2.1 The crystalline cellulose of *Valonia ventricosa*

Commercially available cellulose, Avicel PH-101, is derived from wood products and comes in the form of particles 20-100um in diameter. Due to the harsh treatments to extract and create this polydisperse powder, there is a high degree of heterogeneity in this carbon source. The avicel degree of polymerization (~ 200 glucose units before a chain break) is lower than many native celluloses, and after treatment its crystallinity is reduced to only 50% [61]. Furthermore, the large particle size causes light scattering under a microscope and prevents efficient image acquisition. Avicel also displays some autofluorescence and this interferes with the imaging of other fluorescent particles concurrently viewed (data not shown). Consequently, this cellulose source is not ideal for microscopy experiments monitoring fluorescently labeled cellulases on their substrate.

Valonia ventricosa is a bubble algae known to contain high amounts of type Iα cellulose in its cell wall. Cellulose crystallinity in this organism can exceed 98%, and is thus one of the most crystalline celluloses known [62]. Its cellulose also exhibits high degrees of polymerization, up to several thousand glucose units long [63]. As a result, this cellulose type was pursued for microscopy studies. Bubble algae were collected from various points on the California coast, as well as from local aquariums and other dealers (Figure 2-2, top panels). After ethanol extraction, the cell wall was purified by boiling in 0.1 N NaOH for 5 hours followed by immersion in 0.05 N HCl at room temperature for 12 hours. The results were 'bubbles' that now appeared white in color due to the extraction of all other bioorganic material. These specimens could then be cut and placed on a slide as a sheet of pure cellulose (Figure 2-2, bottom panels) or could be converted into microcrystals for fluorescence microscopy. *Valonia ventricosa* microcrystals were formed by acid hydrolysis in 40% Sulfuric Acid at 70 °C for 12 hours with stirring. The microcrystals were collected by centrifugation, and had a length of several micrometers and a thickness of 20 – 100 nm, as seen by brightfield microscopy. The average degree of polymerization ranged from 300 – 600, as determined by a BCA assay [61].

2.2.2 Preparation of *T. reesei* Cellobiohydrolase I

Cellobiohydrolase I was isolated from the Novozymes Celluloclast mixture using a combination of anion exchange chromatography and gel filtration (Figure 2-3). A first pass over a 16/10 Q Sepharose HP column yielded a few fractions in which

cellobiohydrolase activity could be detected with a MULac assay [94]. These turned out to be mixtures of Cellobiohydrolase I and II and thus additional purification was necessary. A Mono Q 10/100 GL anion exchange chromatographic step was used next. CBH I and CBH II in *T. reesei* are both variably glycosylated [49] making their resolution tricky; consequently, gel filtration with an S-100 Sephacryl column was finally used for separation of these two enzymes. The identity of CBH I was confirmed with mass spectrometry and no CBH II peptides were found.

CBH I was then N-terminally labeled with Alexa fluor 488 using a PLP-mediated reaction [64]. Over 70% was labeled, as determined by absorbance at 488nm. The fluorescent conjugate was tested against the unlabeled protein for cellulase activity on both avicel and valonia cellulose (Figure 2-4). During the first six hours of hydrolysis, the activities of labeled and unlabeled CBH I were comparable.

2.2.3 Tracking of Cellobiohydrolase I on *Valonia ventricosa* cellulose microcrystals

Many enzyme systems are too complex to fully understand through the use of conventional ensemble techniques. Tracking one molecule at a time can reveal deeper insight to the behavior of these enzyme systems [65-67]. Under the right conditions, these molecules can be observed for extended periods of time with high resolution. Total internal reflection fluorescence (TIRF) microscopy was used for the imaging of fluorescently CBH I on cellulose. A suspension of 0.2% (w/v) *V. ventricosa* microcrystals was applied to a quartz slide for 15 minutes. The slide was washed with Sodium Acetate (NaOAc) buffer pH 5 to remove microcrystals that did not adhere to the slide surface. Labeled CBH I concentrations of 2-20 pM in NaOAc buffer pH 5 were then added to the cellulose and a cover slip was placed on top and sealed with an epoxy resin to initiate the reaction. TIRF microscopy enables the illumination of only ~100nm beyond the slide-solution interface [68]. Thus only a very thin layer of the reaction on the slide was observed, which is essential to eliminate the background of emissions by any contaminants. To accurately observe single molecules, high efficiency optical detection and strong signal-to-noise ratios are demanded. Both prism-based and objective lens TIRF configurations of the microscope were tested, with the latter yielding better detection plus the added convenience of being able to modify the microscope configuration after imaging had begun. An Olympa 100x (1.45NA) objective lens, an Andor iXon EMCCD camera (90% quantum efficiency), and a Coherent CW Sapphire laser at 488nm was used for detection. This configuration yielded an effective pixel size of 80-100 nm. The temperature of the stage could be heated to 40C to incubate the reaction without too drastically affecting image quality.

A wide-field view of labeled CBH I on *V. ventricosa* cellulose is shown in Figure 2-5A. The enzymes localized to cellulose and nonspecific binding elsewhere was not observed. Due to comparison of images of microcrystals without enzyme added, these are likely labeled enzymes and not contaminants. A photobleaching profile was conducted of the fluorophore alone in these conditions, and most were able to withstand 150-200 exposures without photobleaching. The exposure time per image was reduced to 50 ms or less, with x-y second intervals between images, so that many frames could be taken. Imaging over many intervals is necessary because the action of cellulases can be slow, delayed, and irregular. However, lowering the exposure time also reduces the photon count captured per frame, which can affect tracking resolution. Different

frame intervals were tested to capture different time scales of cellulase action, but all movies were completed within the first 6 hours of incubation. Under these conditions, we tracked Cellobiohydrolase I on cellulose microcrystals. A moving cellulase can be observed in Figure 2-5B. Over the course of several seconds, a labeled enzyme travels in a linear fashion over 300nm.

2.2.4 Trajectories of Cellobiohydrolase I

We have traced the trajectories of hundreds of enzymes using the methods described above. A sampling of enzymes on a cellulose microcrystal is shown in Figure 3-6. Here many different behaviors of Cellobiohydrolase I can be seen. Some enzymes remain apparently stationary for over an hour, while some show different types of movements. For example, a labeled enzyme might move nonlinearly (most often randomly) and then remain stationary for an extended time. Or, an enzyme might be moving linearly (presumed processive action on cellulose), pause for a period of time, and then start to move according to 2-D surface diffusion models. Thus, there exist a great variety of behaviors of cellulases on the surface of cellulose.

To generate trajectories for CBH I, we adapted custom software in IDL to fit a 2-dimensional Gaussian curve to the point spread function of fluorophores in every frame [65]. The approximate localization of the enzyme can be determined beyond the full width at half maximum if the photon count is high enough and the peak of this Gaussian curve can be isolated with low enough uncertainty [69, 70]. Based on our S/N ratio of approximately 15, we achieved ~20nm resolution while tracking Cellobiohydrolase I.

The behaviors of CBH I seen here are varied and can be classified into a few distinct populations (Table 2-1). Given our spatial resolution of 20nm, we determined that imaging should take place at longer frame intervals in order to better capture the motions of CBH I over longer periods of time. Thereafter, we imaged every 3 seconds or 30 seconds for 200 frames. The population percentages in Table 2-1 are an average of the behaviors seen at any given point in time for 788 enzymes. The largest population are enzymes that land on cellulose but within a couple frames disappear, thus were termed “transient” enzymes. Surprisingly, a large percentage of enzymes appear stationary on cellulose; however, whether they are productively or unproductively bound is unclear. And, as previously mentioned, there are smaller populations of moving CBH I, in either a linear or nonlinear manner. We suggest these cellulases are processively acting on cellulose (linear movement) or searching for a free chain end (nonlinear movement). An independent means of measuring enzyme activity would be required to confirm that the moving enzymes are catalytically active.

2.2.5 Cellobiohydrolase I on Endoglucanase-Pretreated Cellulose

Endoglucanases act synergistically with CBH I by creating more free ends for the exoglucanase to operate on [17]. This can be seen in bulk enzyme assays (Figure 2-7). The soluble sugars released from CBH I and Endoglucanase I (EG I) together were greater than the amount released by CBH I alone plus EG I alone. To a lesser extent, pretreatment of cellulose with an endoglucanase also increased CBH I hydrolysis. We sought to perform microscopy experiments to characterize the enhanced activity of CBH I. Due to endoglucanase action, CBH I was more productive; therefore the population of enzymes on cellulose should be shifted to more productive states. Because

endoglucanses in the reaction may interfere with tracking and complicate observations, we sought to observe CBH I on EG I-pretreated cellulose. The experiments were conducted as before except with the substitution of endoglucanase-pretreated *Valonia ventricosa* microcrystals for the untreated substrate.

The results are shown in Table 2-2 for 718 enzymes. As expected, the percentage of transient and nonlinear CBH I enzymes decreased, and the population of linearly moving cellulases increased. Surprisingly, the population of stationary enzymes grew significantly, suggesting that apparent non-mobile behavior may still be productive action on cellulose. Several possibilities may explain this observation. For example, the stationary enzymes may be struggling to feed a glucan chain into their active site and only eventually hydrolyze cellulose processively, but not within our limits of spatial resolution. They may also be binding, hydrolyzing, and then dissociating and rebinding, acting more like a distributive enzyme, whose action is localized due to the CBM anchoring it in place. Though productive enzymes are in this population, there may also be nonproductive cellulases among them. Preliminary experiments in buffer at pH 7 (where both catalytic aspartates in CBH I are deprotonated—activity is abolished, but the folded protein is still stable [71] (Clark Lab, data unpublished)) show that, on endoglucanase-pretreated cellulose microcrystals, the linearly moving enzyme population is eliminated but the stationary enzyme population looks similar (data not shown). These results would suggest that the linearly moving group is catalytically active and that the stationary group contains some nonproductive enzymes as well.

2.2.6 AFM Imaging of the *Valonia ventricosa* Cellulose Surface

Complementary to tracking CBH I on its substrate, we also characterized the cellulosic surface with AFM imaging after enzyme treatment. An example is shown in Figure 2-8 using *Valonia ventricosa* cell wall cellulose (not microcrystals). Before treatment with CBH I, both microfibrils and macrofibrils can be seen, the latter being weaved into a rough lattice in the algal cell wall. The cellulose was treated with *T. reesei* CBH I in NaOAc buffer pH 5 for 24 hours at 50 °C. The remaining cellulose was imaged under similar tapping mode conditions on the Veeco Bioscope II AFM with silicon cantilevers. After digestion, nearly all cellulose ultrastructure was lost (Figure 2-8B).

Over 30 images were taken for both CBH I-treated and untreated cellulose. A summary of surface trends are shown in Table 2-3. During hydrolysis, micro- and macrofibrils are smoothed out by the action of CBH I over 24 hours. The height range, RMS roughness, and surface area are all reduced as well. These findings describe that over the course of hydrolysis with CBH I, the cellulose surface becomes more flat and topographically less varied, and that cellulose surface features can provide accessible binding sites for degradation.

The effect of ionic liquids on *V. ventricosa* cellulose was also examined with AFM imaging. Ionic liquids, or molten salts, are capable of dissolving cellulose, and are considered by some to be a possible cellulose pretreatment in biofuel production before enzymatic depolymerization [72]. 1-butyl-3-methylimidazolium chloride was used to dissolve *V. ventricosa* cellulose. Water was added to precipitate the polysaccharide and the particles were imaged under similar tapping mode conditions (Figure 2-9). It is apparent that this ionic liquid converts the crystalline structure of the *V. ventricosa* cell

wall lattice into an amorphous solid, thereby helping to explain why ionic liquid-treated cellulose is easier for cellulases to digest [72].

2.3 Conclusions

The interactions of cellulases with their substrate are complex and not well understood. Here, we have characterized the movements of Cellobiohydrolase I on cellulose using single molecule fluorescence microscopy. Protocols for using *Valonia ventricosa* as a cellulose source were developed, and on this substrate a number of CBH I behaviors were observed. A majority of enzymes during a hydrolysis reaction only transiently interact with cellulose. A large population remains stationary, and smaller groups move both linearly and nonlinearly. Over the course of a cellulase's lifetime, the enzyme will display a number of these varied behaviors.

Linear moving cellulases are presumed to be acting processively along a glycan chain, at a rate of approximately 10.4 nm/s. At the time of these experiments, these were the first direct observations of CBH I moving on cellulose of which we knew. A velocity of 10.4 nm/s is slightly higher than expected, though in the correct approximate range, given the kcat of CBH I on cellohexaose is 9.5 nm/s [74]. However, processivity rates could be higher on cellulose than activity on soluble cellodextrins, due to additional binding contacts made with a full glycan chain in the active site. It is also possible that if a chain was highly extracted from the rest of the cellulose crystal, that the energy of hydrolysis could help drive the enzyme forward along a glycan chain, making the enzyme appear to move faster. This possible mechanism might also explain why occasionally CBH I produces cellotriose and cellotetraose [21, 22], rather than exclusively cellobiose. However, it should be noted that our estimate of CBH I velocity is biased toward enzymes that are capable of moving distances greater than 20nm (our limit of resolution). Enzymes acting processively whose motions we were not able to capture, due to their shorter distances, might also be moving more slowly. Thus increasing our spatial resolution will be an important improvement moving forward. Recently, High Speed (HS)-AFM was used to monitor CBH I on pure cellulose [99]. Though the technique was different, their average rates are similar to the speeds we found. For CBH I, they observed an average rate of 7.1nm/s, in the same approximate range as our measurements, with a few enzymes moving as fast as 24nm/s. Their time resolution is not yet high enough to capture the catalytic step of one cellobiose cleavage, so these estimates might be refined again in the future (See also Section 4.2). Nevertheless, these data shed some light on the processive nature of *T. reesei* Cellobiohydrolase I.

In addition to the linearly moving cellulases, we also observed enzymes moving nonlinearly on cellulose. Some movements could be approximately fit with 2-D Brownian motion models, and these are considered to be cellulases diffusing on the surface of cellulose searching for a free chain end. Some moved less randomly, though these may also be searching for a free chain end, with their movement likely guided by surface features of the cellulose. These features could include surface roughness or changes in the orientation of surface glycan chains, for example. Surface abnormalities may cause some directions of movement to be energetically less favorable than they would be on a pristine cellulose surface. Thus surface heterogeneity likely affects not only hydrolysis rates and the distances CBH I is able to move, but also the time before it

finds a free chain end. Others have also proposed that processivity and surface dynamics are substrate-limited [75, 99].

Interestingly, the stationary cellulases observed on the surface of crystalline cellulose likely contain both productive and nonproductive enzymes. When endoglucanase-pretreated cellulose is used, a substrate on which CBH I is more active, we see a larger population of cellulases in the stationary state. We speculate the productive fraction of these enzymes may be struggling to extract a glycan chain from the rest of the cellulose crystal, and do not hydrolyze enough sugars to be detectable within our limits of spatial resolution. This suggests that many active cellulases hydrolyze fewer than 20 cellobiose units on *V. ventricosa* microcrystals before either dissociation or inactivation. The degree of processivity of CBH I has been estimated on multiple substrates by various methods [58-60], with average estimates ranging from 5-85 cellobiose units [58-60]. We see the longest distances travelled in the 250-300nm range, and predict many are below 20nm. In the HS-AFM study, no distribution of distances was given but the traces shown range from 40 to 70nm. Therefore it seems that greater temporal and spatial resolution is still needed to understand the processive capabilities of CBH I.

Lastly, AFM was used to characterize the changes in cellulose after CBH-I or ionic liquids treatment. The enzyme was found to have a peeling effect on the microfibrils and macrofibrils of cellulose in the *V. ventricosa* cell wall, smoothing out these surface features over time. Other groups have observed this effect as well, though with different sources of cellulose [76, 90]. It seems the processive nature of this enzyme causes a slow erosion of the cellulose surface. And as a result of erosion-like degradation, the z range of these images decreases. The RMS roughness and surface area also decrease, indicating that the topographical variability of *V. ventricosa* cellulose decreases over time with CBH I treatment. Ionic liquids also disrupt the structure of *V. ventricosa* cellulose, albeit in a different manner. These liquids are capable of dissolving cellulose, and after treatment with them, a highly crystalline cell wall becomes amorphous and, consequently, much more susceptible to degradation [72].

2.4 Materials and Methods

2.4.1 Preparation of *Valonia ventricosa* cellulose

To acquire *Valonia ventricosa*, ads on Craigslist were posted and local aquariums were contacted, asking for Bubble Algae. These slow-growing algae are seaweeds that often contaminate reef aquariums and other marine tanks. *V. ventricosa* were picked by pressing gently on either side of the firm bubble and slowly twisting off of live rock that had been removed from seawater tanks. They were stored in water until they were cleaned with ethanol in the laboratory. The algae were allowed to sit in ethanol for 30 minutes and then boiled in 0.1 N aq. NaOH for five hours. The cell wall solids were then immersed in 0.05 N aq. HCl at room temperature for 12 hours. After these extractions to remove all other bioorganic material from the algal cell, the remaining cellulose wall appears white (like tiny jellyfish bells) and is stored in water.

The degree of polymerization was determined with BCA and phenol-sulfuric acid assays described in [61].

2.4.2 Preparation of fluorescently-labeled *T. reesei* Cellobiohydrolase I

Cellulclast 1.5L by Novozymes was purchased from Sigma-Aldrich. This broth contains a mixture of secreted proteins as well as sugars and other supernatant compounds. The broth was first concentrated and buffer exchanged using tangential flow filtration with a 10 kDa MWCO PES membrane (Millipore, Billerica, MA) into 25 mM HEPES buffer pH 7.4. The filtrate was then loaded onto a HiLoad 16/10 Q Sepharose column (GE Healthcare) at 5 mL/min. Proteins were eluted from the Q column with a linear gradient from 0 to 0.5 M NaCl over 15 column volumes. Fractions with the highest cellobiohydrolase activity (see below) were pooled and buffer exchanged into 25 mM HEPES buffer pH 7.4. The protein was then loaded onto a MonoQ 10/100 GL column (GE Healthcare) and eluted with a linear gradient from 0 to 0.5 M NaCl over 8 column volumes. Fractions containing cellobiohydrolase activity were pooled and loaded onto a S-100 Sephacryl Gel Filtration column at a rate of 1mL/min. CBH I elutes after the CBH II contaminants. The purified CBH I was then concentrated and buffer exchanged into 50mM Sodium Acetate buffer pH 5 with 10 kDa MWCO spin concentrators (Millipore) and stored at -80 ºC.

A fluorometric assay using 4-Methylumbelliferyl-α-D -lactoside (MULac) [94] was used to determine cellulase activity in culture supernatants, similar to previously described methods [95]. Each 100 µL reaction contained 50 µL 1 mM MULac, 1.67 µL 3 M NaAcetate pH 5.0, 28.33 µL H_2O. After the addition of 20 µL culture supernatant, liberation of 4-methylumbelliferone was measured (excitation wavelength= 355 nm and emission wavelength=460 nm) over 10 minutes.

Cellobiohydrolase I was then N-terminally labeled with an Alexa fluor 488 dye as described by [64]. The protein was buffer exchanged into 25mM phosphate buffer pH 6.5 and incubated with a final concentration of 10mM pyridoxal phosphate (PLP) to form a di-ketone at the N-terminus. The PLP was removed through buffer exchange into fresh 25mM phosphate buffer pH. 6.5 and the modified protein was incubated with N-hydroxylamine-Alexa fluor 488 to finally create a CBH I – Alexa fluor 488 oxime conjugate. Free dye was removed with buffer exchange into 50mM Sodium Acetate buffer pH 5. Absorption at 488nm was used to determine the amount of dye in the protein sample, as per the Alexa Fluor dye instructions. Activity of the cellulases was determined with a phenol-sulfuric acid assay described in [73].

2.4.3 Microscopy

In microscopy, Total Internal Reflection (TIR) is attained by directing the light beam to hit an interface between a high refractive index and a low refractive index (e.g. quartz slide and aqueous sample) at a critical angle such that the light is totally reflected back to the direction from which it came, as described by Snell's Law [68]. Though the beam is reflected back completely, an evanescent wave into the low refractive medium is generated from this reflection that decays within 100nm [68]. Thus a very thin layer of the sample is illuminated [68]. Objective-type TIRF microscopy, where the light beam is directed from below the sample through the objective, reflected, and passed back down

through the objective again, was the primary method used in the preceding experiments because it avoids the spherical aberrations associated with prism-based TIRF. In addition, high N.A. oil immersion objectives (NA > 1.45) can be used to obtain higher collection efficiency, producing better resolution, as opposed to water-immersion objectives (N.A. = 1.2) needed to prevent the mismatch of the refractive indices in prism-type TIRF. To efficiently detect emitted photons and minimize the detector noise, a low-noise, back-illuminated EMCCD camera was used.

An Olympus 100x (1.45NA) oil-immersion objective lens was mounted on a nosepiece of an inverted microscope (Zeiss Axiovert 100). The microscope system was set up on an optical table for stability. A laser beam from a Coherent Sapphire CW Laser (488 nm, 500 mW) was attenuated by neutral density filters and then expanded with a 5x beam expander (ThorLabs Inc.) After conversion into circular polarization by a quarter-wave plate (l/4), the laser beam was focused on the back focal plane of the objective for Koehler illumination. The laser beam was then reflected by a mirror and then by a dichroic mirror. Illumination was switched between epi-fluorescence microscopy and objective-type TIRFM by shifting the position of the mirror. The power at the sample was 2 mW to 5 mW in our objective-based TIRF system. 488/520nm excitation/emission (HQ525/50M) filters were used from Chroma. Imaging and photon counting were performed concurrently by splitting the beam with a half mirror. Images were recorded with an Andor Technology EMCCD camera (iXonEM) every 3 seconds with a 1024 x 1024 format. Glass coverslips and Quartz slides (Matsunami, Japan) were cleaned with piranha etching and washed thoroughly with water before use and stored in water. Milli-Q (Millipore, USA) water was used in all the experiments.

2.4.4 Slide preparation and Imaging

A suspension of 0.2% (w/v) *V. ventricosa* microcrystals was set on a quartz slide for 15 minutes. The slide was washed with Sodium Acetate (NaOAc) buffer pH 5 to remove microcrystals that did not adhere to the slide surface. Labeled CBH I concentrations of 2-20 pM in NaOAc buffer pH 5 were then added to the slide with the adherent cellulose, and a cover slip was placed on top and sealed with an epoxy resin to initiate the reaction.

The slide was placed onto the stage and TIRF was generated. The power at the sample was 2 mW to 5 mW with an exposure time of 100ms, and an image was taken every 3 seconds for most time courses; some time courses every 30 seconds were also taken. Our photobleaching experiments (described below) indicated the dye could last approximately 200 frames before photobleaching. After 200 frames, a new microcrystal particle was examined.

Photobleaching of the Alexa Fluor 488 dye was tested by coating the surface of a slide with polylysine, and then adding a 1nM concentration of free dye. Some dye nonspecifically adhered to the polylysine coating. The slide was washed with NaOAc buffer pH 5 several times to remove any free dye and an imaging time course as described above was run to determine the distribution of photobleaching times. A conservative choice of 200 frames was made, where 90% of the dyes were still fluorescing. At 200 frames, the dye lasts for 20 seconds, emitting ~800,000 collected photons before it photobleaches.

It should be noted that given the heterogeneity of how cellulases move on their heterogenous substrate, no one mode of imaging can capture all of the varieties of their motions. For example, if an enzyme is in the act of hydrolysis, ~10 frames per second would be needed to capture each step the enzyme made. But at that imaging rate, another enzyme that was paused in the same frame would likely photobleach before it had the chance to unpause and move linearly or otherwise. Consequently, we opted for slower imaging (every 3s, 30s) in our first attempts to try to capture as many motions as possible over longer periods of time. We chose this approach first, as opposed to using high power for higher photon counts, so that we could prolong photobleaching and see the diversity of movements over time. We did not hold determining the step size of CBH I as the ultimate goal, because we speculated it to be 1nm (the length of cellobiose). However, we also did not expect to see so many stationary enzymes within these limits of resolution. As a consequence of our imaging approach, we are only capable of determining rates for enzymes moving distances longer than 20nm, and did not create a distribution of distances travelled because we knew the data would be skewed by our resolution limits.

2.4.5 Data Analysis

TIRF is a wide-field technique and, as such, each image contained multiple enzymes. Variable-sized binning was done by hand to section a fluorescent molecule from others in the image before Gaussian fitting. For an image collected by a charge-coupled device, the point-spread function (PSF) is not strictly a Gaussian distribution, but rather a Gaussian distribution integrated over each pixel. Thus, knowledge of the effective pixel size is necessary, and with our EMCCD and optic magnification specifications, here it is approximately 100nm. Before the Gaussian fitting, the possible features were found by subtracting the mean pixel value from the image and then locating all pixels greater than a proper threshold in ImageJ software. For each pixel above this threshold, the surrounding area of the image was singled out and determined as the region of the PSF ready for 2D Gaussian fitting.

The 2D Gaussian fitting applied to the PSF was of the general form:

$$I(x, y) = I_{background} + A\exp\left\{-\frac{1}{2}\left[\left(\frac{x - x_0}{s_x}\right)^2 + \left(\frac{y - y_0}{s_y}\right)^2\right]\right\}$$

where I (x, y) is the emission intensity distribution, x_o and y_o are the coordinates of the center, and s_x and s_y are the standard deviations of the distributions in each direction. A simplex algorithm does the fitting with a least-squares estimator, allowing the constant A to float. A partial script (courtesy of Ahmet Yildiz) was modified in IDL for the fitting. The average position, the standard deviation, as well as the standard error of the mean can be determined. [65]

To determine, if an enzyme was stationary, moving linearly or nonlinear, or transient, its average position was compared to the average position of the same molecule immediately before and after. For those deemed linear, the linearity threshold

was determined to be 0.990 or greater. Some of the nonlinear trajectories could be fit to 2-D Brownian motion models in SigmaPlot; other surface diffusion models were not tested. The number of particles determined as stationary, linearly moving, nonlinearly moving, and transient was counted per frame and then summed over all frames. Therefore, if a particle displayed changing behavior, all types of its trajectory would be described.

2.4.6 Endoglucanase-pretreated Cellulose

Endoglucanase I (EG I) was purified from the Novozymes Celluclast 1.5L mixture with the 16/10 Q Sepharose column. The purification is described above and the chromatogram is shown in Figure 2-3. For the pretreatment of *V. ventricosa* cellulose, microcrystals were incubated 50 uM EG I for 24 hours at 50C. The microcrystals were then washed in 10% SDS to remove any remaining enzyme, and then extensively washed in water before being exchanged into 50mM NaOAc buffer pH 5 for assays and microscopy.

The phenol-sulfuric acid assay from above was modified to include additional cellulose to mimic microscopy conditions. The volume in the slide chamber can be approximated (100um x 2cm x 2cm) and after counting the number of cellulose particles observed and projecting their volume, we estimate the slide contains 20g/L cellulose. 50uM of each enzyme was still used for each reaction; in the concurrent EG I treatment reaction 50 uM of both CBH I and EG I was used.

2.4.7 AFM imaging

Valonia ventricosa cell wall cellulose was cut with scissors to convert the semi-spherical shape to a flat sheet, and was spread on a glass slide as a single layer of pure, native cellulose. Due to the size of the cellulose sheet, they were manipulated by hand or with tweezers, and do not need to be fixed to the slide. Milli-Q Water was pipetted on top to keep the cellulose wet. Tapping mode was used on a Veeco Bioscope II with Veeco gold-coated silicon nitride SNL probes. A triangular cantilever 120um in length was used, with a nominal spring constant of 0.35N/m and resonant frequency range of 50-80kHz. The probe size was 2nm. The adjacent cantilever was broken off to prevent any interference with imaging. The cantilever was tuned in water, generally around 15kHz. All imaging was conducted in pure Milli-Q water. Images of 512 × 512 pixel were collected over a 500 × 500 nm area. The integral and proportional gains were modulated until the trace and retrace lines matched; the typical scan rate was 0.5 Hz. These images have a dynamic range (along the z direction) of 1μm in an 8-bit format.

2.4.8 Cellobiohydrolase I-treatment of *Valonia ventricosa* cellulose

Valonia ventricosa cellulose was treated with *T. reesei* Cellobiohydrolase I for 48 hours at 50C. Cellulose from 3-5 extracted bubble algae were placed in 5mL of NaOAc buffer with 200uM of purified CBH I. The digested cellulose was imaged as described above.

2.4.9 Ionic liquids-treatment of *Valonia ventricosa* cellulose

For studies with ionic liquid-treated cellulose, cellulose from 10-20 extracted *Valonia ventricosa* bubble algae were immersed in 100 mL of 1-butyl-3-methylimidazolium chloride, purchased from Sigma-Aldrich, and placed in a preheated oven at 120C for 3 hours. To regenerate the cellulose, 5 mL of Milli-Q water was used as an anti-solvent, precipitating the cellulose into polydisperse particles. These particles were then placed on a glass slide but not fixed. The particles were first tested for their positional stability by lowering the cantilever down onto the particle and checking that trace and retrace lines were stable. Stable particles were then imaged as described above.

3. A *Neurospora crassa* Kinase Involved in the Transition to Cellulolytic Metabolism

Partially taken from Zepeda V*, Gunda P*, Wallace IS, Glass NL, and Cate JHD. "A *Neurospora crassa* Kinase Involved in the Transition to Cellulolytic Metabolism." (Manuscript in Preparation)

3.1 Cellulase Induction and Transcription Factor Activation – the Search for Signaling Molecules

In order to break down and consume cellulose, *Neuropora crassa* must recognize the presence of its substrate and signal to produce enzymes for cellulose degradation. Studies in our lab have suggested that *N. crassa* has a specific system of induction for cellulases. As compared to those on sucrose, *N. crassa* cultures grown on cellulose (Avicel) were found to have significantly higher levels of cellulase expression and secretion through combined transcriptome/secretome analysis [48]. Subsequent RNA deep sequencing used for transcriptional profiling revealed that, when *N. crassa* was grown in the presence of cellulose as its sole carbon source, the most highly induced cellulases showed a mapped read ratio of up to 10,000 rpkm on avicel, with very few reads on sucrose (C. Haussman and W. Beeson, unpublished data). These results and others have led to a proposed model for cellulase induction by *N. crassa* (Figure 3-1A) [48]. A basal level of cellulases and other enzymes are first produced to scavenge for possible lignocellulosic sources. In the absence of readily available glucose [42], these in turn generate soluble inducer molecule(s) from cellulose that then signal for the upregulation of cellulase gene expression.

In addition to degradative enzymes, a number of predicted sugar transporters are also induced during growth on cellulose [48]. Work in our lab was conducted to elucidate their role in cellulose degradation and these proteins were found to be high-affinity cellodextrin transporters [77]. These transporters, with the help of intracellular β-glucosidases, enable *N. crassa* to consume sugar in the form of cellodextrins and thereby create a new path for sugar to enter the cell. Because cellodextrins can be directly transported, it is possible they also function as signaling molecules. Several transcription factors have also been identified as integral components of cellulase induction. When these transcription factors are deleted, cellulase transcription in *N. crassa* is drastically reduced (N. Louise Glass Lab, unpublished data).

Kinase enzymes are frequently involved in the transmission of signals and control of complex processes *in vivo*. Moreover, transcription factor activation is often achieved via phosphorylation, which may involve an entire upstream signaling cascade [40]. Thus a more detailed model for cellulase induction is proposed here (Figure 3-1B). Signaling molecules derived from lignocellulose enter the cell and through one or more kinases signal to activate transcription factors for the transcription of cellulase genes. A screen of over one hundred *N. crassa* deletion strains of kinase, phosphatase, and other putative signaling enzymes genes was conducted to identify potential members of the cellulose-induced signaling pathway.

3.2 Results and Discussion

3.2.1 Screening *N. crassa* Knockout Strains for Cellulose-specific Phenotypes

Neurospora crassa knockout (KO) strains [46] for over 100 kinase, phosphatase, GPCR, and other possible signaling proteins were acquired from the Fungal Genetics Stock Center (FGSC) and propagated on sucrose slants according to standard protocols [45, 78]. To determine if these genes are involved in cellulose utilization by *N. crassa*, liquid cultures of each deletion strain were grown and compared to wild type (WT) *N. crassa*. The strains were grown on both Vogel's sucrose media and Vogel's cellulose (Avicel) media in order to identify cellulose-specific phenotypes. Cultures were observed visually for growth defects, and protein secretion and supernatant endoglucanase activity were monitored with Bradford and Azo-CM-cellulose assays, respectively.

Most strains showed either no phenotype on either carbon source, or deleterious effects on both sucrose and avicel. A few strains showed a slight improvement in protein secretion and endoglucanase activity; however, their activity was enhanced over WT by less than 1.5-fold. Consequently, this stimulation was not considered significant. Seven strains displayed a strong cellulose-specific response. These strains were classified as potential regulators of cellulose degradation and are listed in Table 3-1 with their predicted protein classification. Of these seven strains, ΔNCU07399 (FGSC#17963) was the most severely impaired and was chosen for further characterization. As shown in Figure 3-2, over seven days of growth this strain accumulated almost no fungal biomass and could not robustly degrade cellulose.

3.2.2 Phenotypic Characterization of ΔNCU07399

Wild type *N. crassa* was typically grown up to two days on Vogel's sucrose media and seven days on Vogel's Avicel media without nutrient limitation. After 48 hours on sucrose, ΔNCU07399 and WT *N. crassa* looked relatively similar (Figure 3-2) with an extensive network of mycelia filling each flask. On avicel, WT *N. crassa* also produced an extensive network of mycelia, but turned orange (a starvation response [39] indicating that cellulose is difficult to degrade), and after seven days degraded the provided cellulose into soluble sugar. In contrast, ΔNCU07399 formed a compact mat of fungal biomass and consumed almost no cellulose. When grown on avicel, in addition to the unusual morphology, ΔNCU07399 secreted over 10-fold less protein than WT after seven days (Figure 3-3). Similarly, the endoglucanase activity of the mutant strain supernatant was reduced more than 10-fold relative to WT, and was only detectable after seven days (Figure 3-3).

When grown on solid sucrose media, ΔNCU07399 showed stunted growth of aerial hyphae as well as low conidiation levels (Figure 3-4). To better understand the mutant's impaired growth on sucrose, the rate of mycelium extension was measured in solid sucrose media race tubes. ΔNCU07399 had a growth rate approximately 80% of that of WT (Figure 3-4). Although ΔNCU07399 grew somewhat less robustly on sucrose relative to WT, its growth defect was still considered to be cellulose-specific due to the severity of its phenotype on this carbon source. A complemented strain

showed WT-like secretion levels and activity, signifying the strain's impaired growth is due solely to the deletion of NCU07399 (Figure 3-5).

3.2.3 Transcriptional Induction of Cellulase Genes in ΔNCU07399

The role of NCU07399 in cellulase regulation was further probed to determine if this enzyme controlled the transcription of cellulases. Since WT *N. crassa* significantly upregulates cellulase RNA transcript levels when N. crassa is grown on cellulose sources, qPCR was first used to determine if ΔNCU07399 is able to similarly induce cellulases. Cultures of each strain were grown on sucrose media for 16 hours, washed, and transferred to Avicel or sucrose media. After four hours, RNA was extracted from the mycelia and prepared for qPCR analysis. As expected, WT *N. crassa* grown on Avicel showed an immense induction of tested genes relative to the sucrose control samples, with the relative quantification (RQ) of each gene averaging between 1700 and 22,000 (Figure 3-6). In comparison, ΔNCU07399 showed a fairly weak but still quantifiable induction of cellulase transcripts (RQ = 43-650).

Transcriptional upregulation levels on cellulose, relative to basal levels from growth on sucrose, show dramatic differences between the two strains for each of the five enzymes examined (Figure 3-6). The two major cellulases, Cellobiohydrolase I (CBH I) and Cellobiohydrolase II (CBH II) were induced approximately 30-fold less in ΔNCU07399 compared to WT. Endoglucanase II (EG II) and β-glucosidase upregulation levels were reduced approximately 15-fold and 5-fold, respectively. Strikingly, upregulation levels of Glycoside Hydrolase 61 (GH 61) were ~50-fold lower than in WT (Figure 3-6). Thus the reduced protein secretion of ΔNCU07399 and lower cellulase activity of ΔNCU07399 grown on avicel is due primarily to a lack of cellulase transcriptional activation.

3.2.4 The Secretion Capability of ΔNCU07399

The above results show that ΔNCU07399 is quite impaired in transcribing cellulase mRNAs as a response to cellulose. Low extracellular protein levels are at least in part due to a lack of transcriptional activation. However, this does not rule out an additional role of NCU07399 in controlling the secretion of expressed cellulases. In order to test whether this putative kinase also regulates the secretion of cellulases, cultures were grown on Vogel's BSA media. It has been shown that *N. crassa* is capable of growing on protein as a carbon source, so long as a low concentration of sugar is initially added to commence growth [87]. Under these conditions, *N. crassa* secretes proteases, which can be detected by SDS-PAGE and can be analyzed using a standard azo-casein assay. This method of growth was used to establish if ΔNCU07399 is incapable of secreting enzymes in general or if the defect is specific to cellulases. WT and ΔNCU07399 *N. crassa* strains were grown on Vogel's media with 1% BSA and 0.1% sucrose, and samples were collected after 24 and 48 hours. By SDS-PAGE, the secretion profiles of the two samples were similar after 24 hours and almost identical after 48 hours (Figure 3-7A). An azo-casein assay to measure protease activity of the samples found very similar activity profiles for the WT and ΔNCU07399 *N. crassa* strains as well (Figure 3-7B). This indicates that ΔNCU07399 is able to respond to and degrade carbon sources other than carbohydrates. Thus, the deletion of NCU07399 does not cause a general secretion defect.

3.2.5 Secretion Profile of ΔNCU07399

Though ΔNCU07399 does not have a general secretion defect, there are few cellulases secreted into its supernatant. In addition to having less protein in the supernatant, the proteins found extracellularly are also different from those secreted by wild type *N. crassa* (Figure 3-8). WT and ΔNCU07399 *N. crassa* were grown on 2% avicel for seven days just as in the growth characterization experiments. Supernatant samples were collected, filtered, and concentrated 10-50 fold and analyzed by SDS-PAGE (Figure 3-8). Protein bands were then excised, trypsin digested, and submitted for Mass Spectrometry analysis. As expected, a number of bands found in the WT secretion profile but not found in the deletion strain supernatant included various cellulases (e.g. GH6, GH61 family members). Interestingly, though, there were a few proteins found in the deletion strain supernatant that are not well represented in the WT secretion profile. These include an arabinofuranosidase (NCU02343) and, most notably, a metalloprotease (NCU07200).

The presence of this metalloprotease in large part may explain the dearth of cellulases in the culture supernatant, in addition to the lack of transcriptional activation. While cellulase transcription may be reduced 10-50 fold, this response was detected after four hours of incubation with cellulose. In contrast, protein and cellulase activity often cannot be detected in the supernatant until after 5-7 days. There are at least two possible non-mutually exclusive explanations for this discrepancy. Supernatant cellulases first bind to cellulose and therefore the very low level of enzymes secreted were trapped on avicel and eluded detection in the supernatant until a threshold level of protein was secreted. Secondly, the significant presence of this metalloprotease may suggest that cellulases were being digested in the supernatant and possibly being reused as a food source. Notably, this protease is not part of *N. crassa*'s general stress response (P. Benz, unpublished data), suggesting that its expression is a specific defect of ΔNCU07399 deletion.

3.2.6 ΔNCU07399 Induction Response to Cellobiose

The current model for cellulase induction in *N. crassa* requires that a basal level of cellulases be expressed in order to produce an inducer molecule [48]. Therefore the inability of ΔNCU07399 to efficiently degrade cellulose could be due to its failure to produce scavenger cellulases that release an inducer molecule. Alternatively, it is possible that even when presented with a potential inducer, ΔNCU07399 would still be unable to upregulate cellulase genes. To distinguish between these two possibilities, ΔNCU07399 was grown on cellobiose in the presence of a β-glucosidase inhibitor.

Studies with *T. reesei* have used a β-glucosidase inhibitor (nojirimycin) to block the production of sophorose and prevent cellulase induction [86]. Our lab has previously shown that cellobiose can act, though to a lesser extent than crystalline cellulose, as an inducer of cellulases when the action of extracellular β-glucosidases is blocked (Figure 3-9, and J. Galazka and E. Znameroski, unpublished data). By preventing cellobiose breakdown into glucose outside of the cell, glucose repression is partially relieved and an upregulation of cellulase transcripts is observed. Therefore,

WT and ΔNCU07399 were grown on 2% sucrose for 18 hours, washed, and transferred to either 2% Avicel, 2% cellobiose, or 2% Cellobiose + Nojirimycin. A MuLac activity assay [94] using culture supernatants from 24-hour cultures showed that supernatant from WT *N. crassa* grown on cellobiose + nojirimycin had about 20% of the exoglucanase activity of Avicel grown cultures (Figure 3-10). Almost no detectable activity was observed in WT samples grown on cellobiose, due to the strong effects of glucose repression in the presence of an active β-glucosidase.

By contrast, there was no MULac activity in any of the ΔNCU07399 cultures. By collecting total RNA 4 hours after the transfer from sucrose, qPCR analysis of several cellulase genes showed no significant increase in transcript level as well (Figure 3-11). The only gene that showed a slight induction was an intracellular β-glucosidase gene (NCU00130, RQ =9), which was probably due to the increase in cellobiose inside the cell. This strongly suggests that the absence of cellulase activity in the ΔNCU07399 strain is not simply due to the failure to produce scavenger cellulases because, even when more cellobiose is allowed to enter the cell and glucose repression is relieved, ΔNCU07399 still does not upregulate cellulase genes.

3.2.7 *In vivo* Expression and Localization of NCU07399-GFP

NCU07399 wildtype and kinase dead (KD) constructs were prepared in the pNeurA-GFP vector [96] and transformed into *N. crassa*. Mycelia from transformants grown on sucrose were visualized using standard brightfield microscopy and appeared normal and healthy. By epifluorescence, the GFP tagged constructs were easily visualized indicating the protein was well expressed (Figure 3-12). Samples were also analyzed by confocal microscopy, using both mycelia from liquid cultures as well as germinated conidia on agar plates after 16 hours. Confocal microscopy revealed a diffuse localization as well as punctate accumulations throughout the mycelia (Figure 3-13). The localization of wild type NCU07399 and the KD mutant was similar. The punctate spots do not overlay with *N. crassa* nuclei, nor are they aggregates of cleaved GFP (data not shown). Colocalization experiments labeling parts of the endocytic pathway, secretory pathway, and other known markers will be required to identify the possible organelle to which NCU07399 associates.

3.2.8 *In vitro* Expression, Purification and Activity of NCU07399

An *E. coli* codon optimized NCU07399 gene was cloned into an expression vector for *in vitro* expression and purification (see Materials and Methods). The construct (7399-pGEX2T) was prepared with both an N-terminal GST tag and a C-terminal 6x-His tag to aid in purification. An additional construct was prepared with the predicted catalytic aspartate (residue 238 mutated to an alanine to create 7399KD-pGEX2T, a putative kinase dead/inactive version of NCU07399. After transforming *E. coli* cells with these constructs, the kinases were expressed under standard conditions (see Materials and Methods) and lysates were purified using a Ni-NTA column. The eluate from the first purification step was applied to a glutathione sepharose column, but protein was not recovered from this column (Figure 3-13A). An anti-His Western blot revealed that the major band in the eluate from the Ni-NTA column was the recombinantly expressed protein that ran at ~72 kDa, the expected size of the putative kinase with both a His and GST tag attached (Figure 3-13).

After purification of the NCU07399 wild type and kinase dead constructs, each sample was used in an autophosphorylation assay to test for *in vitro* activity. Protein samples were incubated with γ-[^{32}P]-ATP in the appropriate buffer and reactions were visualized by autoradiography. Phosphorylation activity was seen in the NCU07399 wildtype kinase sample, but not in the D238A mutated construct (Figure 3-14). This indicates that NCU07399 is indeed a kinase, and that its catalytic residue was correctly predicted. Of note is the high molecular weight band present in the kinase sample that is heavily phosphorylated. Mass spectrometry has identified NCU07399 as the primary component of the band, suggesting that this kinase may be capable of oligomerizing. Lastly, NCU07399 was also found to be capable of trans-phosphorylating myelin basic protein, further validating its kinase activity (Figure 3-15).

3.2.9 Bioinformatic and Phylogenetic Analysis of NCU07399

BLAST analysis of the NCU07399 amino acid sequence identified homologs in many related cellulolytic fungi, such as *Podospera anserina* and *Chaetomium globosum* (Table 3-2). NCU07399 is predicted to be a kinase in the serine/threonine protein kinase 16 (STK16) type. STK16 has human, mouse, yeast, and plant members [80, 81] and belongs to the NAK family of kinases which show great structural diversity and low sequence homology with other protein kinases, even in generally conserved sequences like the nucleotide binding motif [82]. This group of kinases, and NCU07399 in particular, seems to have unique characteristics that set them apart from typical kinases.

The activity of protein kinases is usually regulated by altering the conformation of the activation loop, a 20-35 residue sequence bridged by a DFG—APE motif [83]. Phosphorylation of residues in the activation segment generally causes the unstructured loop to become structured, resulting in the formation of substrate binding sites. Preliminary mass spectrometry results show that NCU07399 has both common autophosphorylation sites in its activation loop, as expected, as well as an autophosporylation site outside of this region (Figure 3-16). Furthermore, in addition to abnormal phosphorylation sites, this activation loop may also be structured even before phosphorylation. MPSK1 (myristoylated and palmitoylated serine/threonine kinase 1) is the human homolog of NCU07399 and the only STK16 with an available structure. It was found to have an atypical activation segment with a β-sheet and a large α-helical insertion [84].

NCU07399 has an additional 100 amino acids in comparison to MPSK1 and these are mainly found within two insertions. In the primary structure the additional residues are on either side of the catalytic region and activation loop (Figure 3-16, dashed lines in MPSK1 sequence). A homology model of NCU07399 was made and shows the same structured activation loop as MPSK1 (Figure 3-17, red). The two insertions in the NCU07399 model are shown in blue and yellow, with the first containing some helical structure and the second modeled as a random coil. While NCU07399 probably adopts a structure similar to MPSK1, it is unclear how the additional sequences in the kinase might affect substrate binding and activity.

While NCU07399 only has 34% sequence identity with MPSK1, much of the conservation can be found in regions such as the activation, catalytic, and nucleotide binding regions (Figure 3-16). This includes the atypical activation loop as well as the

conserved DLG, rather than the standard DFG, motif at the start of the region. Lastly, as the name suggests, MPSK1 has N-terminal consensus sequences for myristoylation (Cys6) and palmitoylation (Cys8) [85]. These two cysteines in the N-terminal region of NCU07399 might be targets for these post-translational modifications, which may be responsible for the localization seen in the confocal microscopy images (Figure 3-13).

3.3 Conclusions

Neurospora crassa has recently emerged as a system to study cellulose degradation and many new aspects of its cellulolytic system have been discovered. However not much is known about the process by which *N. crassa* senses a solid carbon source – cellulose – and subsequently coordinates a large induction of the genes necessary to break down and use this substrate. The initial screen presented here was aimed at discovering signaling proteins involved in this process. It yielded several interesting strains and phenotypes (Table 3-1), the most severe of which was ΔNCU07399, the deletion strain of a protein kinase. This strain exhibited almost no growth on Avicel and was unable to break down cellulose.

While this strain has no general secretion defect, its ability to transcriptionally upregulate cellulases as a response to cellulose is drastically diminished, in some cases as much as 30- or 50-fold. The deletion of the NCU07399 kinase also allows for a metalloprotease to become highly induced. This protease may impede cellulolysis by degrading cellulases already secreted into the culture supernatant, possibly for its own consumption. Thus it is likely that this kinase controls multiple cellular processes, not just cellulose degradation. A further indicator of this hypothesis includes that it has direct orthologs in several other non-cellulolytic species (Figure 3-18). In these other species, the NCU07399 ortholog is not involved in cellulose degradation, and therefore has other functions. It is possible that these other functions are also controlled by NCU07399 in *N. crassa.* Studies with the direct ortholog deletion strain in the cellulolytic fungus *Aspergillus nidulans* are underway for comparison.

Future work with this kinase will need to include efforts to identify both its substrates as well as its upstream regulators. Other kinases identified in our screen with strong phenotypes might be players in a cascade of regulation that includes NCU07399. Double KO mutants will be made with these strains and ΔNCU07399 to see if they are in the same or in separate pathways. A first contender for this epistasis analysis would be ΔNCU00188 (Table 3-1). As for the final downstream activator, the transcription factors found by the Glass lab to directly induce cellulases may well be the immediate target of this kinase. Biochemical studies will be conducted toward answering this question. In addition, future work regarding NCU07399 will involve modification at the kinase's autophosphorylation sites. For example, aspartate and glutamate can act as phopho-serine mimics [89] and point mutations substituting these residues might create a constitutively active kinase. Development of a hyperactive kinase could yield cellulase overexpression, or possibly even the induction of cellulases in the absence of cellulose. Thus finding cellulase regulators and understanding how they work has the potential to enable manipulation of *N. crassa* for increased and better controlled enzyme production.

3.4 Materials and Methods

3.4.1 *Neurospora Crassa* Strains and Other Resources

All strains were obtained from the Fungal Genetic Stock Center (FGSC) [78] [45]. The strain designated as WT is FGSC 2489. PCR primers were synthesized and purified using standard desalting by IDT DNA Technologies. PCR reactions were carried out using Phusion polymerase (Finnzymes), except in the case of TAIL-PCR when Taq polymerase was used. Sequence alignments were performed using BLAST and ClustalW [91]. Homology models were created using the I-Tasser server for 3D protein structure prediction [92, 93] and rendered using PyMOL (The PyMOL Molecular Graphics System, Version 1.3, Schrödinger, LLC).

3.4.2 Growth Media and Inoculation

For the production of conidia on slants/flats and growth of mycelia in liquid cultures, Vogel's media supplemented with 2% sucrose was used, unless otherwise noted. For slants, 2 mL of 50x Vogel's solution (prepared according to the FGSC) was mixed with 2 g sucrose and 2 g agar per 100 mL. The solution was heated with stirring and then 3 mL aliquots were distributed among culture tubes. After autoclaving for 15 minutes, the tubes were tilted on their sides, cooled to harden, and stored at 4 °C. Flats were prepared in the same manner except 100 mL of the agar solution was placed in a 500 mL flask, autoclaved and set on the bench top to harden before storage or inoculation. A small amount of conidia (frozen or fresh) was placed on the agar media using a sterile wooden stick and grown for 2-3 days in the dark at 30 °C and then placed at room temperature in the light for at least 4 days before use. Liquid cultures (100 mL) were prepared with 2 mL 50X Vogel's solution and 2 g sucrose or Avicel. To inoculate, conidia from slants or flats were resuspended in water and added to liquid cultures to a starting OD_{600} of 0.05, unless otherwise noted. Cultures were grown at 25 °C with constant shaking (200 RPM) and light.

Sucrose race tubes were prepared according to a protocol from the FGSC (http://www.fgsc.net/fgn42/white.html) and kept in the dark (30 °C) to avoid circadian rhythm effects. The farthest distance traveled by mycelia was measured at corresponding time points and plotted to compare the slopes.

3.4.3 DNA extraction

DNA was extracted from conidia (7-28 days old) grown on 2% sucrose slants or from fresh mycelia. 400 µL of lysis solution (0.05 M NaOH, 1 mM EDTA, 1% Triton-X 100) was placed in a 2 mL screw cap tube, with ~0.3 g of 0.5 mm silica beads. A small (pea-sized) amount of conidia or mycelia were placed in the tube and the sample was shaken in a bead beater twice in 1 minute intervals. The sample was placed in a 65 °C water bath for ten minutes, inverting 2-3 times during the incubation to mix. After the addition of 80 µL of 1M Tris pH 7.5, samples were centrifuged at maximum speed in a bench top centrifuge (5 minutes) and the supernatant was removed. An equal volume of phenol-chloroform was added, samples were inverted to mix and then centrifuged again for 10 minutes. The aqueous phase was transferred to a new tube with 600 µL ice-cold ethanol and placed at -20 °C for at least one hour. After precipitation, the

sample was centrifuged for 10 minutes at 4 °C and the pellet was washed with 75% ethanol. The pellet was resuspended in 50-250 µL water or TE Buffer.

3.4.4 Total RNA extraction

Liquid nitrogen frozen conidia or mycelia (~100 mg) were added to a 2 mL screw cap tube with ~0.25 g of silica beads and 1 mL Trizol reagent (Sigma). Samples were vortexed for 3 x 30 seconds, waiting 30 seconds between each round. The tubes were shaken gently for 5 minutes at room temperature and then centrifuged at 13,000 x g for 15 minutes at 4 °C. The supernatant was placed in a new tube, 0.5 mL isopropanol was added and the samples were inverted to mix before placing at -20 °C for at least 2 hours. The isopropanol precipitated samples were centrifuged (13K x g, 4 °C, 10 min) and the pellet was washed with 0.5 mL 75% ethanol. The pellet was allowed to air dry and then 50-250 µL RNase free water was added. To fully dissolve the pellet, the sample was placed at 55 °C for ~10 minutes and flicked several times to mix. After measuring the concentration of the RNA, up to 10 µg was removed and treated with Ambion TURBO DNase (0.5 µL 10x Buffer, 0.5 µL DNase, sample and water to 50 µL) by incubating at 37 °C for 15 min. An extra 0.5 µL of DNase was added and the sample was incubated for another 30 minutes and then the enzyme and buffer was removed using the Qiagen RNeasy RNA clean-up kit. After elution, the RNA concentration was measured and samples were stored in ~500 ng aliquots at -20 °C for short term storage or -80 °C for long term storage.

3.4.5 cDNA synthesis and qPCR

Reactions containing total RNA samples (500 ng, unless otherwise indicated) were setup using the High Capacity cDNA Reverse Transcription Kit (Applied Biosystems) according to manufacturer instructions. The cDNA was diluted 1/10 and qPCR reactions were prepared using the Power SYBR green PCR master mix (Applied Biosystems). Reactions were performed in triplicate and contained 300 nM each forward and reverse primer and 0.2 µL of the diluted cDNA reaction in a total volume of 10 µL. The forward and reverse primers used for qPCR analysis were as follows:

Table 3-3 Genes and primers used for qPCR analysis

Gene Name (NCU#)	Fwd Primer (5'-3')	Rev Primer (5'-3')
Actin	TGATCTTACCGACTACCT	CAGAGCTTCTCCTTGATG
CBHI (NCU07340)	ATCTGGGAAGCGAACAAAG	TAGCGGTCGTCGGAATAG
CBHII (NCU09680)	CCCATCACCACTACTACC	CCAGCCCTGAACACCAAG
Endoglucanase 2 (NCU00762)	GAGTTCACATTCCCTGACA	CGAAGCCAA CACGGAAGA
GH61 (NCU07898)	TCAAGCCCGGTTACTATC	AACCTGTCACCTGCAACT
β-Glucosidase (NCU00130)	GTTCGGCGTTACCTATGT	AGAGTCAAAGAGCGGCTTC

Data Analysis was performed in StepOne Software (Applied Biosystems) using Relative Quantitation/Comparative CT (ΔΔCT). Data was normalized to the endogenous control

(actin) with expression on sucrose as the reference sample. Error bars indicate a 95% confidence interval.

3.4.6 Azo-carboxymethylcellulose (Azo-CMC) Assay

For a standard assay, 200µL Azo-CMC, 40µL 1 M sodium acetate, pH 5.0, 50µL culture supernatant, and 110µL H_2O were incubated at 37°C for 10 minutes. Precipitation buffer (1 mL) was added, the sample was vortexed to mix, and centrifuged at 4000 RPM for 5 minutes. After pelleting the precipitated CMC, the absorbance of the supernatant was read at 590 nm. Precipitation buffer was prepared according to manufacturer's instructions by dissolving 40 g sodium acetate trihydrate and 4 grams zinc acetate in 150 mL water and adjusting to pH 5.0 with 5 M HCl. The solution was brought to 200 mL, mixed with 800 mL 95% ethanol and stored at room temperature until use.

3.4.8 Standard Transfer Experiments

Conidia were inoculated on 2% sucrose media (see above) and grown for 16 hours. Cultures were vacuum filtered and scraped with a sterile spatula into a flask with fresh media. Flasks were placed back at 25°C, 200 RPM shaking in the light for four hours and then collected by vacuum filtration and quick frozen in liquid nitrogen for RNA extraction.

3.4.9 Nojirimycin Transfer Experiments

Cultures were inoculated on 2% sucrose media and grown for 18 hours before being transferred to 0.2% cellobiose, 0.2% cellobiose + nojirimycin, or 0.2% Avicel. Samples were taken after 4 hours for RNA extraction and subsequent qPCR analysis or after 24 hours for an exoglucanase (MULac) assay, described below. Nojirimycin was used at a final concentration of 20 mg/L.

A fluorometric assay utilizing 4-Methylumbelliferyl-α-D -lactoside (MULac) [94] was used to determine cellulase activity in culture supernatants, similar to previously described methods [95]. Each 100 µL reaction contained 50 µL 1 mM MULac, 1.67 µL 3 M NaAcetate pH 5.0, 28.33 µL H_2O. After the addition of 20 µL culture supernatant, liberation of 4-methylumbelliferone was measured (excitation wavelength= 355 nm and emission wavelength=460 nm) over 10 minutes and the slopes of the resulting curves were plotted in comparison to WT *N. crassa*.

3.4.10 Growth on BSA and Azo-Casein Assay

Cultures were inoculated on 1x Vogel's medium with 0.1% sucrose and 1% BSA (added after autoclaving) and grown for 48 hours. Supernatant samples were collected at 24 and 48 hours for SDS-PAGE analysis. To assay non-specific proteases, an azocasein assay was performed according to manufacturer's instructions (Sigma). Briefly, 2.5% (w/v) azocasein was dissolved in 0.5% (w/v) sodium bicarbonate pH 8.3 (at 37 °C). In a reaction tube, 2.5 mL of the azocasein solution was preheated to 37 °C with 1.5 mL of bicarbonate buffer. After equilibration, 1 mL of the sample supernatant was mixed into the solution and incubated at 37 °C for 1 hour. A 1 mL aliquot was removed and added to 4 mL of a 5% v/v TCA solution, mixed, and placed over a 0.45

μm syringe filter. A 1 mL aliquot of the filtered solution was added to 3 mL of a 500 mM NaOH and the absorbance was recorded at 440 nm.

3.4.11 *E. coli* cloning and expression of NCU07399

The nucleotide sequence of NCU07399 was codon optimized for expression in *E. coli* by DNA2.0 (Menlo Park, CA), with the following sequence:

E. coli codon optimized NCU07399 (NCU07399EC)

ATGGCGCAAGTCGTTTCTGACTTCATTTACTGGCTGGGTAACTGTATGGTGTGCTTCCCGGGTAGCC
CGACCCTGAAAATCAACAATCGTAGCTTTAAGATTCTGCGTCTGCTGGGTGAGGGCGGCTTTAGCTA
TGTGTACCTGGTTCAGGATACGAGCACCAGCGAGCTGCTGGCTTTGAAAAAGATCCGCTGCCCGTTT
GGCCAGGAGAGCGTGGCTCAGGCGATGCATGAGGTCGAAGCGTACAAAATCTTCGGCAATACGCC
GGGTATTATCCACCACGTTGACTATAGCATTGCAACCGAACGCGGCAGCGAAGGTCAAGATAAGAC
CGTGTACGTGTTGCTGCCGTATTACCGTCGTGGTAACCTGCAAGACATGATTAATGCGAATCTGGTC
AATCATACCCGCTTTCCGGAGAAACGCCTGATGATGTTGTTCCTGGGTGTCTGCAAGGCCCTGCGC
GGTATGCACAAGTACAAAGGTGGCGCTGGCGGTGACACCAGCGGTGAGTCCATGGAAGTGCCGGG
TGCAGCTGGTAAGCGTAAGAGCAAAACGCGTCAGGCAGCCGTCGGCGGTGCGGATGAGGATGATG
AAACCGAGCAACAGGTGCCACTGATCGAAGAGGAAGGCCGTCTGCCAGGCAGCGGCGAAACGCGC
AGCTATGCGCACCGCGATATCAAACCGGGTAACATCATGATTTCTGACAGCGGTCGTGATCCGATTC
TGATGGACCTGGGTTCCATCGCAGTTTCCCCGCTGCCTATTACGTCGCGCAGCCTGGCGATTGCGA
CTCAGGACACCGCAGCAGAGCATAGCACCATGCCTTACCGTGCCCCGGAACTGTTCGATGTAAAAA
CCGGCACGATTATCGACACCAAGGTCGATATCTGGAGCCTGGGTTGCACGCTGTACGCGTGCCTGG
TTGGCAAGAGCCCGTTTGAGATGCGCAGCGACGAAACGGGCGGTAGCCTGTCTATTTGTGTCTTGT
CCGGTGACTGGCGTTTCCCGGATGAGGGTCCGGGTCAAACCAAGGGCAAAGGTAAAGCGGGTGCC
GGTGGTGGCGCAGGTGGCGATTCCACCGCGACCAACAAAGACGACGAGAACTATATCAGCGAGCC
GATCCGTGACGTTGTTCGTCGTTGTTTGCGTGTTGAACCGGCCGAACGTCCGGACATCGATGAATTG
ATTGAGCTGGTTGAGCGTGTGGTGGAAGAGCTGCCGGAGGACACTGCG

The gene was cloned into the pGEX2T vector, which contains a N-terminal GST tag, between the BamHI and EcoRI sites, with the reverse primer adding a 6x-His tag. The kinase-dead (KD) mutant was produced using a Quikchange protocol (Qiagen) which generated an Asp to Ala mutation at amino acide position 238.

Primer Name	Sequence (5'-3')
7399-pgex2tECfw	GAGCGGATCCATGGCGCAAGTC GTTTCTGACTTC
7399-pgex2tECrv	CGTGAATTCGTGGTGATGGTGATGATGCGCAGTGTCCTC CGGCAGC
7399EcOptKDFw	CTATGCGCACCGCGCAATCAAACCGGGTAAC
7399EcOptKDRev	GTTACCCGGTTTGATTGCGCGGTGCGCATAG

The resulting vectors, 7399-pGEX2t and 7399KD-pGEX2t, were transformed into *E. coli* BL21(DE3) cells (Invitrogen) for expression. Single bacterial colonies containing NCU07399 wild-type or kinase dead mutant encoding plasmids were used to inoculate 20 mL of LB-ampicillin broth and grown at 37 °C for 16 hours with shaking. These cultures were used to seed 1 L of LB-ampicillin broth and the new cultures were grown at 37 °C until they reached an OD_{600} of between 0.6-0.8. The cultures were induced with 0.5 mM IPTG at 37 °C for 4 hrs, and the cell mass was collected by centrifugation at 4000 x g for 15 min at 4 °C. The pellets were frozen at -80 °C until further use.

3.4.12 NCU07399 purification from *E. coli* and *in vitro* activity assays

Bacterial pellets were resuspended in 40 mL of extraction buffer (20 mM Tris-HCl pH 7.5, 300 mM NaCl, 10 mM $MgCl_2$, 20 mM imidazole, Roche complete protease

inhibitor tablet), and lysed with three passes through an Avestin Emulsiflex C3 homogenizer. Insoluble debris was removed by centrifugation at 100,000 x g for 1 hr at 4^0 C, and the clarified extract was loaded onto a 1 mL Ni-NTA agarose column (Qiagen) equilibrated in wash buffer (20 mM Tris-HCl pH 7.5, 300 mM NaCl, 10 mM $MgCl_2$, 20 mM imidazole). The columns were washed with 500 mL of wash buffer, and eluted in a total of 10 mL of Ni-NTA elution buffer (20 mM Tris-HCl pH 7.5, 300 mM NaCl, 10 mM $MgCl_2$, 350 mM imidazole). The purity of the recombinant proteins was assessed by SDS-PAGE.

Protein kinase assays were performed in 50 µL reactions containing kinase buffer (25 mM MOPS-NaOH pH7.0, 10 mM $MgCl_2$, 100 µM ATP, 500 dpm/ pmol γ-[^{32}P]-ATP) and were initiated upon the addition of 1 µg of purified recombinant protein kinase. Samples containing 5 µg of myelin basic protein (Calbiochem) were also included to assay transphosphorylation. Samples were incubated at 37^0 C for 30 minutes, and the reactions were terminated by the addition of 10 µL of SDS sample buffer. 25 µL aliquots of each sample were separated on a 10% SDS-PAGE gel that was subsequently stained with Coomassie blue, destained, and dried. The radiolabeled bands were imaged by autoradiography.

3.4.13 NCU07399 cloning, native expression and native purification

The pNeurA vector [96] was used for cloning (standard ligation-independent cloning method [38]) NCU07399 behind the ccg promoter with a C-terminal GFP tag, allowing for recombination into the his-3 locus. For complementation and other analyses, NCU07399 was cloned into several varieties of the pBC-phleo vector [97], kindly provided by the Glass Lab at UC Berkeley. The pBC-phleo1 vector was created using primers 7399Phleo1Fw and 7399Phleo1Rv to PCR amplify a section of the genome 1116 bp upstream and 236 downstream of the NCU07399 start and stop codon. Two versions of the pBC-phleo vector with a ccg promoter, multiple cloning site, and encoding a GFP or dsRed C-terminal tag were termed pBC-phleo2 and pBC-phleo3, respectively. Primers were designed to clone NCU07399 into the multiple cloning site of each vector using the XbaI and BamHI sites (7399Phleo2Fw/Rv) or the SpeI and XbaI sites (7399Phleo3Fw/Rv). All constructs were amplified from gDNA using standard protocols.

Construct	Fw Primer (5'-3')	Rev Primer (5'-3')
7399-Phleo1	GCTAAAGCTTCAACTGTTGTGC GGGTACCTTG	TAGAGTGGGAACACATGACAA AGC AGTG
7399-Phleo2	GCTATCTAGAATGGCGCAAGTA GTT TCAGAC	TAG CGG ATC CAG CGG TAT CTT CGG GCA ACT CC
7399-Phleo3	GCTAACTAGTATGGCGCAAGTA GTT TCAGAC	TAGCTCTAGATCAAGCGGTATC TT CGGGCAAC

Conidia (400 µL of solution with an OD_{600} equal to 100) were used to inoculate a 2 L unbaffled flask containing 1 L of liquid Vogel's with 2% Sucrose media. Cultures were grown for 48 hours at 25 °C in the light with constant shaking (200 RPM) and then harvested by filtering over miracloth. The fungal pellet was squeezed to remove excess media and allowed to sit in 1 L Millipore water to resuspend. Cultures were filtered over miracloth a second time and then resuspended in 1 L Vogel's acetate media. The

washed and resuspended cultures were grown for another 48 hours in the conditions listed above. Mycelia were harvested by filtering cultures over a glass microfiber filter using a Buchner funnel. After the first filtration step, mycelia were collected and dried by vacuum filtration over a 0.2 µm PES filter and frozen in liquid nitrogen.
Frozen mycelia were ground to a fine powder under liquid nitrogen using a mortar and pestle. The powder was ground with lysis buffer (10 mM Tris pH7.5, 250 mM NaCl, 0.05% Triton X-100, 10 mM Imidazole, Roche complete Protease Inhibitor tablet) and insoluble debris were removed by centrifugation at 6000 x g for 15 minutes. Lysates were clarified by an additional centrifugation step for 20 minutes at 27000 x g and passing over a 0.2µm PES syringe filter. The clarified lysate was loaded on a 5 ml Ni-NTA HisTrap HP column (GE Healthcare) pre-equilibrated in lysis buffer.

3.4.14 SDS PAGE, Western Blot, and Antibodies

Unless otherwise noted, 10% Criterion precast Tris-HCl SDS-PAGE gels were run at 200 V for one hour and stained with Bio-Safe coomassie stain, both available from Bio-Rad. After transferring to a nitrocellulose membrane, Western blots were blocked in 5% milk and then incubated with the appropriate primary and secondary antibodies (HRP fusions) before being visualized using 3,3′,5,5′-Tetramethylbenzidine (TMB) Liquid Substrate System for Membranes (Sigma). The primary antibodies used were the His-probe (H-15) rabbit polyclonal IgG (Santa Cruz Biotechnology) for 6x-His tag detection and the anti-GFP Rabbit serum polyclonal (Invitrogen) for GFP.

3.4.15 *N. crassa* transformation

Competent conidia were prepared by harvesting freshly grown spores and resuspending them in 30 mL of ice-cold 1M sorbitol. The conidia suspension was then filtered over cheesecloth and centrifuged at 4C at 3400 rpm for 10 minutes. The conidia were resuspended in 30 mL 1M sorbitol and spun twice more to remove any associated hyphae. The final conidial pellet was resuspended into 1 mL of ice-cold sorbitol and placed on ice. 1 µg of DNA for each transformation was prepared in 10 µL of water. 90 µL of conidia and 10 µL (1 µg) of DNA were placed into pre-chilled cuvettes for electroporation. A negative control of 10 µL of sterile water was used. Each electroporation was done at 1.5 kV, 600 ohms, and 25 µF with a 1 mm gap cell. Immediately after electroporation, 900 µL of 1M ice-cold sorbitol was added to each cuvette and left on ice.

Plates with bottom agar containing 1x Vogel's, 2% agar, and 1x FIGS (1L 10X FIGS contains 200g L-Sorbose, 5g D-Fructose, and 5g D-Glucose) were poured and solidified prior to transformation. Aliquots of 10 mL top agar (1x Vogel's, 1% agar, 1x FIGS) were kept in liquid form at 65 °C for each transformation plate. After electroporation, 50 µL, 100 µL, or 300 µL of conidia were each added to 10 mL of top agar and mixed immediately by inversion. These were each then poured onto plates with bottom agar and allowed to solidify. 3 plates were made for each transformation with varying amounts of conidia (50 µL, 100 µL, and 300 µL). Plates were placed at 30 °C and after 3 days colonies were picked and grown on new slants of 1x Vogel's-Sucrose, 2% agar.

4. Summary and Conclusions

4.1 Understanding the Mechanisms and Production of Cellulases

Fungi are among of the most efficient cellulose degraders known, due to their diverse set of cellulolytic enzymes. They are likewise the most robust producers of cellulases, and improving upon this will be a key step forward to the widespread realization of cellulosic biofuels [8-10]. In fact, enzyme cost has already been identified as one of the main economic barriers to industrial-scale ethanol from plant cell walls [12]. Thus understanding and exploiting the regulation of cellulase production in fungi can yield extensive benefits. In a similar manner, a reduction in enzyme cost can be achieved through the improvement of cellulase action. Understanding how these enzymes can work more productively and for longer periods of time will be wholly valuable.

4.2 Cellobiohydrolase I Processivity and Behavior on a Solid Substrate

Cellobiohydrolase I (CBH I) is a GH family 7 exoglucanase that comprises approximately 60% of secreted *T. reesei* cellulases [54]. It is considered one of the most processive cellulases [57] and displays a number of behaviors while on the surface of cellulose. We have observed distinct modes of action for CBH I on cellulose, including linear movement and stationary pausing, and found an average speed of 10.4 nm/s for the linearly moving enzymes, which we presume to be catalytically active. We have also characterized the surface of cellulose with AFM imaging before and after CBH I and ionic liquids treatment. Since the last of our biophysical experiments described here were performed, new data has arisen that includes observations consistent with our findings. In 2009, Igarashi *et. al.* observed the processivity of *T. reesei* CBH I on crystalline cellulose with high speed (HS) atomic force microscopy, and found an average rate of 3.5 nm/s [98]. The catalytic domain alone could travel at velocities similar to the full-length protein, though these events occurred much less frequently likely because, without its CBM domain, a given enzyme cannot readily find a chain end [98].

Earlier this year, they also made further observations about the behavior of cellulases on cellulose. In the 2011 study, CBH I enzymes travelled unidirectionally along the crystalline cellulose surface, but would collectively halt in a manner the authors described as similar to a traffic jam [99]. In our work, cellulase concentrations were too low for this to occur but their observations are interesting nonetheless. The authors also treated crystalline cellulose simultaneously or separately with *T. reesei* CBH II, and due to synergistic effects the proportion of mobile enzymes increased. These results are similar to those we observed upon pretreating cellulose with EG I. Pretreating the substrate with ammonia (known to swell cellulose) also increased the number of moving cellulases [99]. Thus modifying cellulose with pretreatments (such as ammonia or ionic liquids), predicted to be an important part of its depolymerization in biofuel production [72], correlates with increased cellulase activity on cellulose surfaces. It should be noted that in the second study the average velocity of CBH I was found to be 7.1 nm/s (twice the velocity estimated earlier) and Igarashi *et. al.* speculate it is due

to their averaging of two populations (both moving and stopped enzymes) in the earlier work [92]. Thus the behavior of cellulases on cellulose is complicated, tricky to characterize with more still to be understood. Between this work and ours, it appears that increasing the number of chain ends, as well as disrupting the dense crystallinity of native cellulose through pretreatment, can improve the mobility of cellulases and increase their hydrolytic efficiency.

4.3 Regulating Cellulase Production in *Neurospora crassa*

Neurospora crassa is a well-established model organism that has already been used to study many aspects of fungal biology. This made it an ideal system for studying the complicated processes involved in cellulose degradation and metabolism. We were able to quickly screen through over a hundred knockout strains and identify several genes that could play a role in cellulase production. Moreover, the protein interactions and signaling pathways in *Neurospora crassa* are likely applicable to many other eukaryotes, especially other cellulolytic fungi.

To avoid wasting energy on making unproductive enzymes, *Neurospora crassa* has developed a means to specifically induce cellulases only in the presence of cellulose [48], and in the absence of available glucose [42]. The cellulase system of *N. crassa* is still largely unexplored, but with the genetic tools and enzyme diversity in *N. crassa*, this organism has become a model organism for cellulose degradation, and has the potential to become an industrial microbe as well. The screen presented here of *N. crassa* knockout strains sheds some light on proteins that might be involved in cellulase production. In particular, we identified an STK-16 family kinase, NCU07399, which regulates the transcriptional induction of cellulases in the presence of cellulose.

Regulatory mechanisms in *N. crassa* will likely have relevance in many other organisms, particularly other cellulolytic fungi. Comparisons between the ΔNCU07399 strain and the homologous deletion strain from *Aspergillus nidulans (*A1295 *A. nidulans* KO ANID_10193.1) are currently being performed. If the *A. nidulans* kinase knockout strain also shows a cellulose specific growth defect, this will indicate that the function of this kinase is conserved in other fungi and further establish the relevance of *N. crassa*'s cellulolytic system.

Future work with this kinase will also include efforts to identify its substrates and upstream regulators. Other kinases identified in our screen with strong phenotypes might be players in a cascade of regulation that includes NCU07399. Therefore double knockout strains will be made to determine either new pathways controlling cellulase production, or new components of the same pathway in which NCU07399 operates. Transcription factors identified by the Glass lab to directly induce cellulases are suspected final targets of the NCU07399's regulation. *In vitro* studies will be conducted to see if any of them are phosphorylated by our kinase. In addition, future work will involve the re-engineering of NCU07399's activation loop. We hope to make point mutations at its autophosphorylation sites [89] to attain constitutive NCU07399 activity. Development of a hyperactive kinase could yield cellulase overexpression, or possibly even the induction of cellulases in the absence of cellulose. This could have great potential for biofuels production because it might enable cellulase expression without actually needing cellulose, and therefore reduce the cost of enzyme production. Thus

finding cellulase regulators and understanding how they work is an important step toward the realization of widespread cellulosic biofuels.

References

1. Lehninger, A.L., D.L. Nelson, and M.M. Cox, *Lehninger principles of biochemistry*. 4th ed. 2005, New York: W.H. Freeman. 1 v. (various pagings).
2. Somerville, C., et al., *Toward a systems approach to understanding plant cell walls.* Science, 2004. **306**(5705): p. 2206-11.
3. Carpita, N. and C. Vergara, *A Recipe for Cellulose.* Science, 1998. **279**(5351): p. 672-673.
4. Perez, J., et al., *Biodegradation and biological treatments of cellulose, hemicellulose and lignin: an overview.* International microbiology : the official journal of the Spanish Society for Microbiology, 2002. **5**(2): p. 53-63.
5. Farrell, A.E., et al., *Ethanol can contribute to energy and environmental goals.* Science, 2006. **311**(5760): p. 506-8.
6. Ragauskas, A.J., et al., *The path forward for biofuels and biomaterials.* Science, 2006. **311**(5760): p. 484-9.
7. O'Sullivan, A. C. *Cellulose: The Structure Slowly Unvravels.* Cellulose, 1997. **4**: p.173-207.
8. Lynd, L., R. Elamder, and C. Wyman, *Likely features and costs of mature biomass ethanol technology.* Applied biochemistry and biotechnology, 1996. **57-58**(1): p. 741-761.
9. Bisaria, V.S. and T.K. Ghose, *Biodegradation of cellulosic materials: Substrates, microorganisms, enzymes and products.* Enzyme and Microbial Technology, 1981. **3**(2): p. 90-104.
10. Lynd, L.R., C.E. Wyman, and T.U. Gerngross, *Biocommodity Engineering.* Biotechnology progress, 1999. **15**(5): p. 777-793.
11. Lynd, L.R., et al., *Microbial cellulose utilization: fundamentals and biotechnology.* Microbiology and molecular biology reviews : MMBR, 2002. **66**(3): p. 506-77.
12. Himmel, M.E., M.F. Ruth, and C.E. Wyman, *Cellulase for commodity products from cellulosic biomass.* Current opinion in biotechnology, 1999. **10**(4): p. 358-64.
13. Stephanopoulos, G. *Challenges in Engineering Microbes for Biofuels Production.* Science, 2007. **315** (5813): p. 801-804.
14. Baldrian, P. and V. Valaskova, *Degradation of cellulose by basidiomycetous fungi.* FEMS microbiology reviews, 2008. **32**(3): p. 501-21.
15. Maki, M., K.T. Leung, and W. Qin, *The prospects of cellulase-producing bacteria for the bioconversion of lignocellulosic biomass.* International journal of biological sciences, 2009. **5**(5): p. 500-16.
16. Valjamae, P. *et. al. Synergistic cellulose hydrolysis can be described in terms of fractal-like kinetics.* Biotechnol Bioeng., 2003. **84**(2): 254-7.
17. Levine, S.E., *et al. A Mechanistic Model of the Enzymatic Hydrolysis of Cellulose.* Biotechnology and Bioengineering, 2010. 107 (1): 37-51.
18. Henrissat, B, et al. *Cellulase families revealed by hydrophobic cluster analysis.* Gene, 1989. **81**: p. 83-95.
19. Cantarel, B.L., et al., *The Carbohydrate-Active EnZymes database (CAZy): an expert resource for Glycogenomics.* Nucleic Acids Research, 2009. **37**(Database issue): p. D233-8.

20. Kubicek, C. P. *The cellulase proteins of Trichoderma reesei: structure, multiplicity, mode of action and regulation of formation.* Advances in Biochemical Engineering and Biotechnology, 1992.
21. Teeri, T. T., et al. *Trichoderma reesei cellobiohydrolases: why so efficient on crystalline cellulse?* Biochem. Soc. Trans., 1998. **26**: p. 173-178.
22. Horn, S. J. et al. *Costs and benefits of processivity in enzymatic degradation of recalcitrant polysaccharides.* PNAS, 2006. **103** (48): p. 18089-18094.
23. Rouvinen, J., Bergfors, T., Teeri, T., Knowles, J. K. C. and Jones, T. A. (1990) Science **249**, p. 380-386.
24. Alisdair B. Boraston, David N. Bolam, Harry J. Gilbert, and Gideon J. Davies. *Carbohydrate-binding modules: fine-tuning polysaccharide recognition.* Biochem J., 2004. **382**: p. 769–781.
25. Nidetzky, B. *et al. Cellulose hydrolysis by the cellulases from Trichoderma reesei: a new model for synergistic interaction.* Biochem. J. (1994) **298**, p. 705-710.
26. Sternberg, David. *β-Glucosidase of Trichoderma: Its Biosynthesis and Role in Saccharification of Cellulose.* Applied and Environmental Microbiology, 1976. **31** (5): p. 648-654.
27. Igarashi, K. *et. al. Cellobiose dehydrogenase enhances Phanerochaete chrysosporium cellobiohydrolase I activity by relieving product inhibition.* Eur. J. Biochem. **253**, 101-106 (1998).
28. Reichenbecher, M. *et. al. Purification and properties of a cellobiose phosphorylase (CepA) and a cellodextrin phosphorylase (CepB) from the cellulolytic thermophile Clostridium stercorarium. Eur.* J. Biochem. **247**, 262-267 (1997).
29. Stricker, A.R., R.L. Mach, and L.H. de Graaff, *Regulation of transcription of cellulases- and hemicellulases-encoding genes in Aspergillus niger and Hypocrea jecorina (Trichoderma reesei).* Applied Microbiology and Biotechnology, 2008. **78**(2): p. 211-20.
30. Davis, R.H., *Neurospora : contributions of a model organism*. 2000, Oxford ; New York: Oxford University Press. xii, 333 p.
31. Lindegren, C., *A six-point map of the sex-chromosome of Neurospora crassa.* Journal of Genetics, 1936. **32**(2): p. 243-256.
32. Davis, R.H. and D.D. Perkins, *Timeline: Neurospora: a model of model microbes.* Nature reviews. Genetics, 2002. **3**(5): p. 397-403.
33. Beadle, G.W. and E.L. Tatum, *Genetic Control of Biochemical Reactions in Neurospora.* Proceedings of the National Academy of Sciences of the United States of America, 1941. **27**(11): p. 499-506.
34. Donaldson LA. *Ultrastructure of wood cellulose substrates during enzymatic hydrolysis.* Wood Science and Technology, 1988. **22**: p. 33–41.
35. Manley RSJ. *Fine structure of native cellulose microfibrils*. Nature, 1964. **204**: p. 1155–7.
36. A.A. Baker, et al. *New Insight into Cellulose Structure by Atomic Force Microscopy Shows the Iα Crystal Phase at Near-Atomic Resolution*. Biophysical Journal, 2000. **79**: p. 1139–1145.

37. White A.R., Brown Jr. R.M. *Enzymatic hydrolysis of cellulose: visual characterization of the process.* Proceedings of the National Academy of Sciences of the United States of America, 1981. **78**(2): p. 1047–51.
38. Aslanidis, C. and de Jong, P. J. *Ligation-independent cloning of PCR products (LIC-PCR). Nucleic Acids Res.,* 1990. **18**(20): p. 6069-74.
39. Estrada, A. F. et al. *The ylo-1 gene encodes an aldehyde dehydrogenase responsible for the last reaction in the Neurospora carotenoid pathway.* Mol Microbiol., 2008. **69** (5): p. 1207-20.
40. Pregueiro, A. M. et al. *The Neurospora Checkpoint Kinase 2: A Regulatory Link Between the Circadian and Cell Cycles.* Science, 2006. **313** (5787): p. 644-649.
41. Gusakov, A. V. *Alternatives to Trichoderma reesei in biofuel production*, Trends Biotechnol, 2011. **29**: p. 419-425.
42. Sun, J. and Glass, N.L. *Identification of the Cre-1 Cellulolytic Regulon in Neurospora crassa.* PLoS One, 2011. **6** (9): e25654
43. Lee I., et al. *Substrate-enzyme interactions in cellulase systems.* Bioresource Technology*,* 1996. **58**: p.163–9.
44. Cambareri, E.B., *et. al. Recurrence of Repeat-Induced Point Mutation (Rip) in Neurospora Crassa.* Genetics,1991. 127(4): 699–710
45. Galagan, J.E., et al., *The genome sequence of the filamentous fungus Neurospora crassa.* Nature, 2003. **422**(6934): p. 859-68.
46. Colot, H.V., et al., *A high-throughput gene knockout procedure for Neurospora reveals functions for multiple transcription factors.* Proceedings of the National Academy of Sciences of the United States of America, 2006. **103**(27): p. 10352-7.
47. Martinez, D., et al., *Genome sequencing and analysis of the biomass-degrading fungus Trichoderma reesei (syn. Hypocrea jecorina).* Nature biotechnology, 2008. **26**(5): p. 553-60.
48. Tian, C., et al., *Systems analysis of plant cell wall degradation by the model filamentous fungus Neurospora crassa.* Proceedings of the National Academy of Sciences of the United States of America, 2009. **106**(52): p. 22157-62.
49. Himmel, M.E., et al., *Biomass recalcitrance: engineering plants and enzymes for biofuels production.* Science, 2007. **315**(5813): p. 804-7.
50. Fox, J.M. *et. al. Initial- and processive-cut products from cellobiohydrolase-catalyzed hydrolysis of cellulose reveal rate-limiting steps and role of companion enzymes.* Biochemistry, Just Accepted Manuscript, November 21, 2011.
51. Koshland, D. E. *Stereochemistry and mechanism of enzymatic reactions*. Biol. Rev. **28**, 416–436 (1953).
52. Vocadlo, D.J. *et. al. Catalysis by hen egg-white lysozyme proceeds via a covalent intermediate.* Nature **412**, 835-838 (2001).
53. Divne, C. *et. al. High-resolution crystal structures reveal how a cellulose chain is bound in the 50 Å long tunnel of cellobiohydrolase I from Trichoderma reesei.* Journal of Molecular Biology, 1998. **275** (2): 309-325.
54. Enari, T. M. & Niku-Paavola, M. L. *Enzymatic hydrolysis of cellulose.* CRC Critical Reviews in Biotechnology, 1987. **5**: 67-87.
55. Teeri, T. *et. al. Trichoderma reesei cellobiohydrolases: why so efficient on crystalline cellulose?* Biochem Soc Trans., 1998. **26**(2): p. 173-8.

56. Boisset C., et al. *Imaging the enzymatic digestion of bacterial cellulose ribbons reveals the endo character of the cellobiohydrolase Cel6A from Humicola insolens and its mode of synergy with cellobiohydrolase Cel7A.* Appl. Environ. Microbiol, 2000. **66**: 1444–1452.
57. Teeri T. T. *Crystalline cellulose degradation: new insights into the function of cellobiohydrolases.* Tibtech,1997. **15**: p. 160–167.
58. Medve, J. *et. al. Hydrolysis of Microcrystalline Cellulose by Cellobiohydrolase I and Endoglucanase II from Trichoderma Reesei.* Biotech. Bioengin., 1998. **59** (5): p. 621-634.
59. Imai, T. *et. al. Unidirectional processive action of cellobiohydrolase Cel7A on cellulose microcrystals.* FEBS, 1998. **432**: p. 113-116.
60. Kipper, K. *et. al. Processive action of cellobiohydrolase Cel7A from Trichoderma reesei is revealed as 'burst'kinetics on fluorescent polymeric model substrates* Biochem. J., 2005. **385**: p. 527-535.
61. Zhang, YHP. and Lynd, L. R. *Determination of the number-average degree of polymerization of cellodextrins and cellulose with application to enzymatic hydrolysis.* Biomacromolecules, 2005. **6**: p. 1510-1515.
62. Gardner, K.H., Blackwell *The structure of native cellulose.* J. Biopolymers, 1974. **13**: p. 1975-2001.
63. Zugenmaier, P. Crystalline cellulose and derivatives: characterization and structures. Springer, 2007. p. 4.
64. Gilmore J.M., *et. al*. *N-terminal protein modification through a biomimetic transamination reaction.* Angew. Chem., Int. Ed., 2006. **45**(32): p. 5307-5311.
65. Yildiz, A., *et. al. Myosin V walks hand-over-hand: single fluorophore imaging with 1.5nm localization.* Science, 2003. **300** (5628): p. 2061-5.
66. Reck-Peterson, S. L. *et al. Single-Molecule Analysis of Dynein Processivity and Stepping Behavior.* Cell, 2006. **126** (2): p. 335-348.
67. Vale, R. D. *et. al*. *Direct observation of single kinesin molecules moving along microtubules.* Nature, 1996. **380** (6573): p. 451-3.
68. Schneckenburger, H. *Total internal reflection fluorescence microscopy: technical innovations and novel applications.* Current Opinion in Biotechnology, 2005. **16**: p. 13-18.
69. Cheezum, M.K. *et al*. *Quantitative Comparison of Algorithms for Tracking Single Fluorescent Particles.* Biophysical Journal, 2001. **81**: p. 2378-2388.
70. Yildiz, A. Selvin, P. R. *Fluorescence Imaging with One Nanometer Accuracy: Application to Molecular Motors.* Acc. Chem. Res., 2005. **38**: p. 574-582.
71. Boer, H. and Koivula, A. *The relationship between thermal stability and pH optimum studied with wild-type and mutant Trichoderma reesei cellobiohydrolase Cel7A.* Eur. J. Biochem, 2003. **270**: p. 841-848.
72. Shill, K. *et. al. Ionic liquid pretreatment of cellulosic biomass: Enzymatic hydrolysis and ionic liquid recycle.* Biotechnology and Bioengineering, 2011. **108** (3): p. 511–520.
73. T. Wood et. al. Methods in Enzymology **160**: p. 87-112.

74. Nidetzky, B., et al. *Hydrolysis of cellooligosaccharides by Trichoderma reesei cellobiohydrolases: experimental data and kinetic modeling.* Enzyme Micro. Technol. **16**: p. 43-52.
75. Kurasin, M. and Valjamae, P. *Processivity of Cellobiohydrolases Is Limited by the Substrate.* Journal of Biological Chemistry, 2011. **286** (1): p. 169-177.
76. Lee I., et al. *The mechanism of cellulase action on cotton fibers: evidence from atomic force microscopy*. Ultramicroscopy, 2000. **82**: p. 213–21.
77. Galazka, J.M., et al., *Cellodextrin transport in yeast for improved biofuel production.* Science, 2010. **330**(6000): p. 84-6.
78. McCluskey, K., A. Wiest, and M. Plamann, *The Fungal Genetics Stock Center: a repository for 50 years of fungal genetics research.* Journal of biosciences, 2010. **35**(1): p. 119-26.
79. Assiotis, M. and Hsu Chen, V. F. Personal Communication, 12/16/2011.
80. Kurioka, K., et al., *Molecular cloning and characterization of a novel protein serine/threonine kinase highly expressed in mouse embryo.* Biochimica et biophysica acta, 1998. **1443**(3): p. 275-84.
81. Stairs, D.B., et al., *Cloning and characterization of Krct, a member of a novel subfamily of serine/threonine kinases.* Human molecular genetics, 1998. **7**(13): p. 2157-66.
82. Chien, C.-t., et al., *Numb-Associated Kinase Interacts with the Phosphotyrosine Binding Domain of Numb and Antagonizes the Function of Numb In Vivo.* Mol. Cell. Biol., 1998. **18**(1): p. 598-607.
83. Nolen, B., S. Taylor, and G. Ghosh, *Regulation of Protein Kinases: Controlling Activity through Activation Segment Conformation.* Molecular Cell, 2004. **15**(5): p. 661-675.
84. Eswaran, J., et al., *Structure of the Human Protein Kinase MPSK1 Reveals an Atypical Activation Loop Architecture.* Structure (London, England : 1993), 2008. **16**(1): p. 115-124.
85. Berson, A.E., et al., *Identification and characterization of a myristylated and palmitylated serine/threonine protein kinase.* Biochemical and biophysical research communications, 1999. **259**(3): p. 533-8.
86. Reese, E. T. *et al*. *Nojirimycin and d-glucono-1,5-lactone as inhibitors of carbohydrates.* Carbohydr. Res., 1971. **18**: 381-8.
87. Drucker, H., *Regulation of exocellular proteases in Neurospora crassa: induction and repression of enzyme synthesis.* Journal of bacteriology, 1972. **110**(3): p. 1041-9.
88. Luo, Z., M. Freitag, and M. Sachs, *Translational regulation in response to changes in amino acid availability in Neurospora crassa.* Mol. Cell. Biol., 1995. **15**(10): p. 5235-5245.
89. Huang W. and Erickson, R. L. *Constitutive activation of Mek1 by mutation of serine phosphorylation sites.* PNAS**,** 1994. **91(**19): p. 8960-8963.
90. Hanley SJ, et al. *Atomic force microscopy of cellulose microfibrils: comparison with transmission electron microscopy*. Polymer, 1992. **33**: p. 4639–42.
91. Thompson, J.D., D.G. Higgins, and T.J. Gibson, *CLUSTAL W: improving the sensitivity of progressive multiple sequence alignment through sequence*

weighting, position-specific gap penalties and weight matrix choice. Nucleic Acids Research, 1994. **22**(22): p. 4673-80.
92. Roy, A., A. Kucukural, and Y. Zhang, *I-TASSER: a unified platform for automated protein structure and function prediction.* Nature protocols, 2010. **5**(4): p. 725-38.
93. Zhang, Y., *I-TASSER server for protein 3D structure prediction.* BMC bioinformatics, 2008. **9**: p. 40.
94. Wang, L.-X., et al., *A fluorometric assay of ceramide glycanase with 4-methylumbelliferyl-lactoside derivatives.* Glycoconjugate Journal, 1996. **13**(3): p. 359-365.
95. Ribeiro, O., et al., *Expression of Trichoderma reesei cellulases CBHI and EGI in Ashbya gossypii.* Applied Microbiology and Biotechnology, 2010. **87**(4): p. 1437-1446.
96. Sun, J., et al., *Expression and characterization of the Neurospora crassa endoglucanase GH5-1.* Protein Expression and Purification, 2011. **75**(2): p. 147-154.
97. Calmels, T., et al., *High efficiency transformation of Tolypocladium geodes conidiospores to phleomycin resistance.* Current Genetics, 1991. **20**(4): p. 309-314.
98. Igarashi, K. et al. *High Speed Atomic Force Microscopy Visualizes Processive Movement of Trichoderma reesei Cellobiohydrolase I on Crystalline Cellulose.* Journal of Biological Chemistry, 2009. **284** (52): 36186-36190.
99. Igarashi, K. et al. *Traffic Jams Reduce Hydrolytic Efficiency of Cellulase on Cellulose Surface.* Science, 2011. **333**: p. 1279-1282.

Figure 2-1. The Active-Site Tunnel of *T. reesei* Cellobiohydrolase I.
X-ray crystal structure of *T. reesei* Cellobiohydrolase I Catalytic Domain with cellohexaose and cellobiose. The catalytic aspartates are rendered in pink and the cellodextrins in green. This structure provides some insight on the action of CBH I. It is suggested that after a glycan chain is thread through the active-site tunnel (from the right) and cellobiose is cleaved, six sugar residues of the glycan chain remain in the tunnel. Once cellobiose is released from the enzyme (on the left), the remainder of the chain can then slide further into the tunnel for another round of hydrolysis [53].

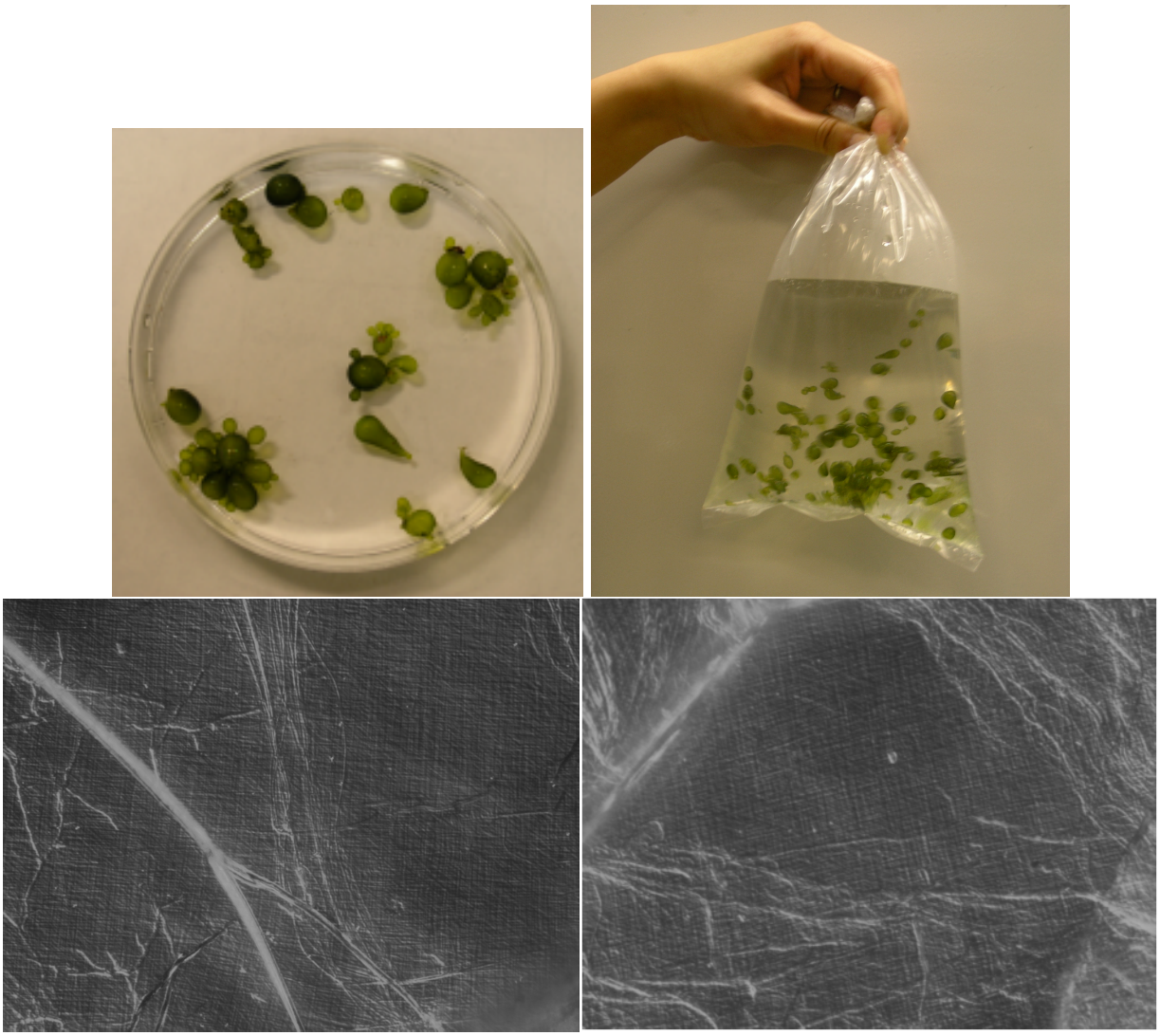

Figure 2-2. The Bubble Algae *Valonia ventricosa* and its cellulose
Valonia ventricosa before extraction (top panels) and brightfield images of its cell wall after mild wash treatments (bottom panels). After extraction, the bubble algae appears white rather than green, as most components other than cellulose have been removed. The lattice features of the remaining cellulose indicate the complex ultrastructure of plant cell walls.

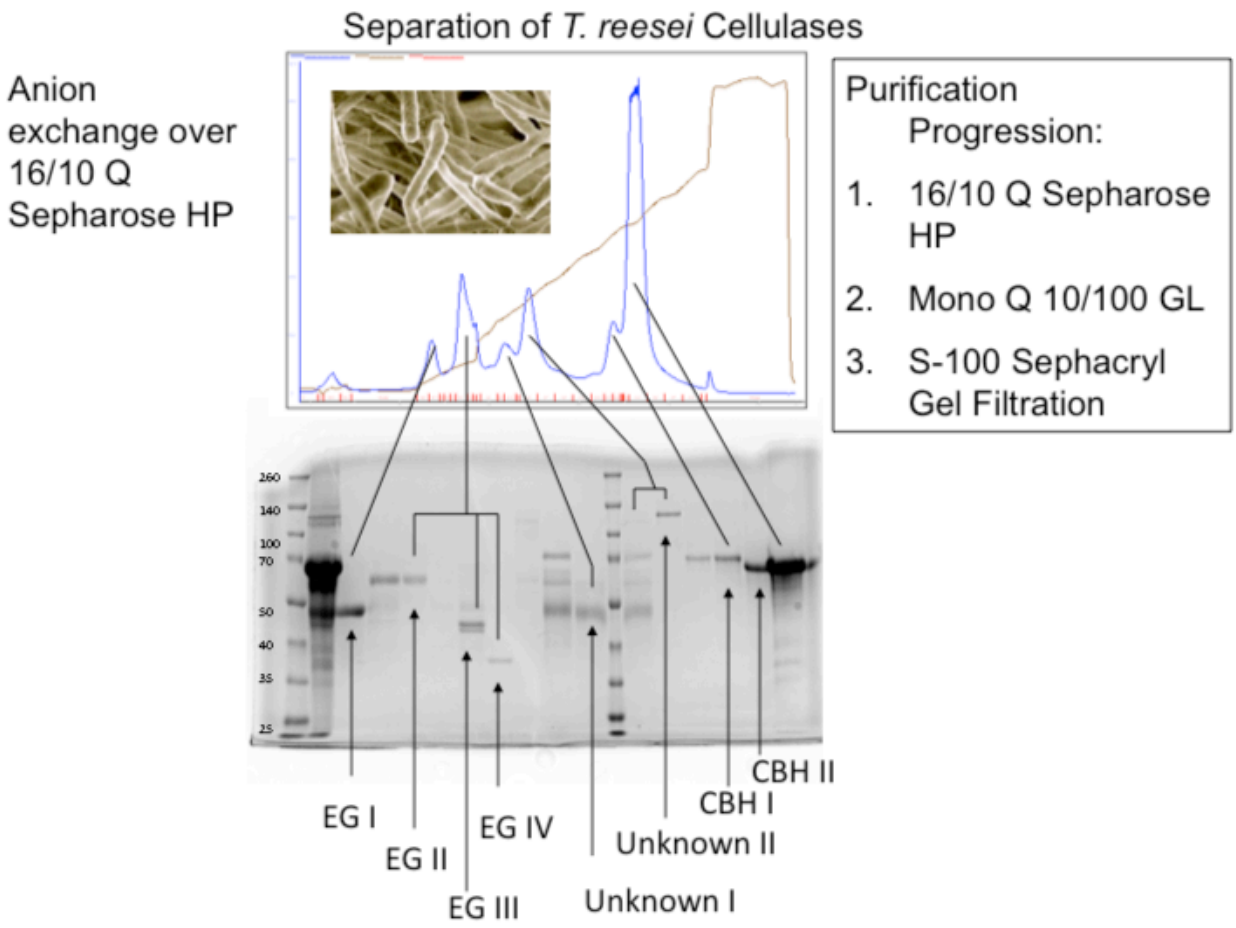

Figure 2-3. Overview of *T. reesei* Cellobiohydrolase I Purification
T. reesei cellulases were obtained from the Novozymes Celluclast mixture and purified with anion exchange and size exclusion chromatography. In order to isolate Cellobiohydrolase I (CBH I), two types of anion exchange were used before gel filtration. Endoglucanases (EG) were removed fairly early, however, additional purification steps were necessary to remove Cellobiohydrolse II (CBH II) impurities. The protein identity was confirmed by mass spectrometry and MULac activity.

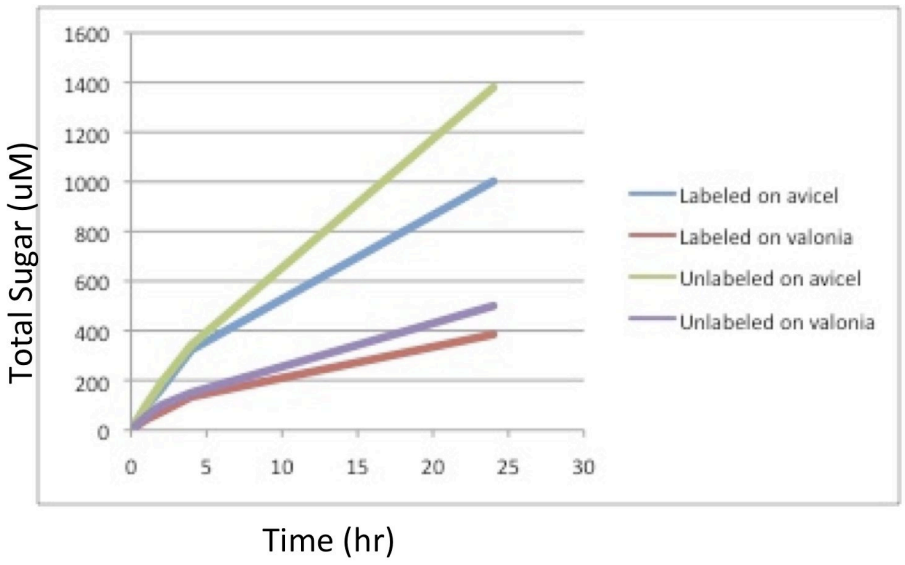

Figure 2-4. *T. reesei* Cellobiohydrolase I Activity on *Valonia* ventricosa cellulose and Avicel.

Total soluble sugar released into solution was measured after CBH I treatment of cellulose. Fluorescently labeled (Alexafluor 488) CBH I was compared with the native enzyme on two substrates. On both avicel and *V. ventricosa* cellulose, an initial burst phase of activity is observed for both enzymes, as is common among cellulases [17]. Though the labeled enzyme shows lower activity after 24 hours, earlier in the reaction the activities are comparable. Consequently, microscopy studies with this fluorescently labeled enzyme were conducted within the first 6 hours of incubation.

A.

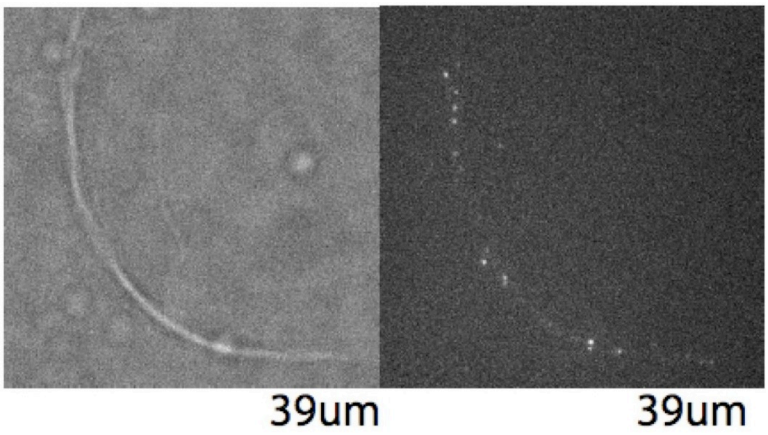

B.

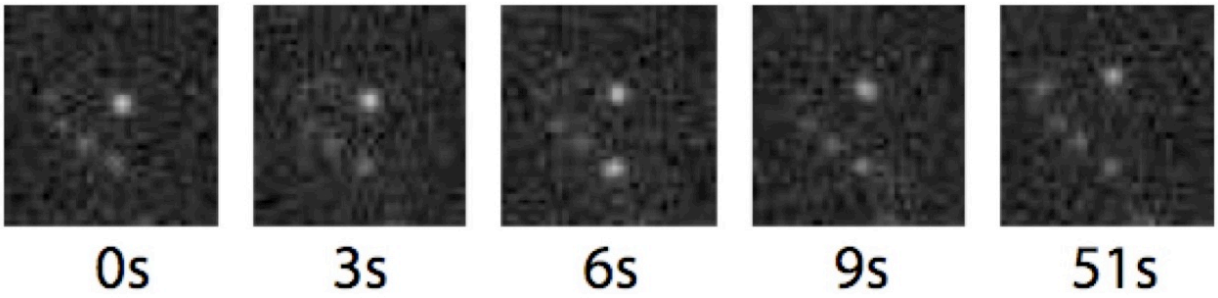

Figure 2-5. Single-molecule Fluorescence Tracking of Cellobiohydrolase I on *Valonia ventricosa* microcrystals.

- **A.** Brightfield (L) and Fluorescence (R) wide-field view of a *V. ventricosa* microcrystal incubated with Alexafluor 488-labeled CBH I. The enzymes localize to cellulose and nonspecific binding elsewhere is not observed.
- **B.** Time course of CBH I on the surface of cellulose microcrystals using Total Internal Reflection Fluorescence (TIRF) microscopy. Four enzymes (on the left) can be observed as stationary on the surface of cellulose. However, a mobile enzyme (right) can be observed linearly advancing along the microcrystal. Gaussian curves were fit to image point spread functions and the peaks were used for tracking.

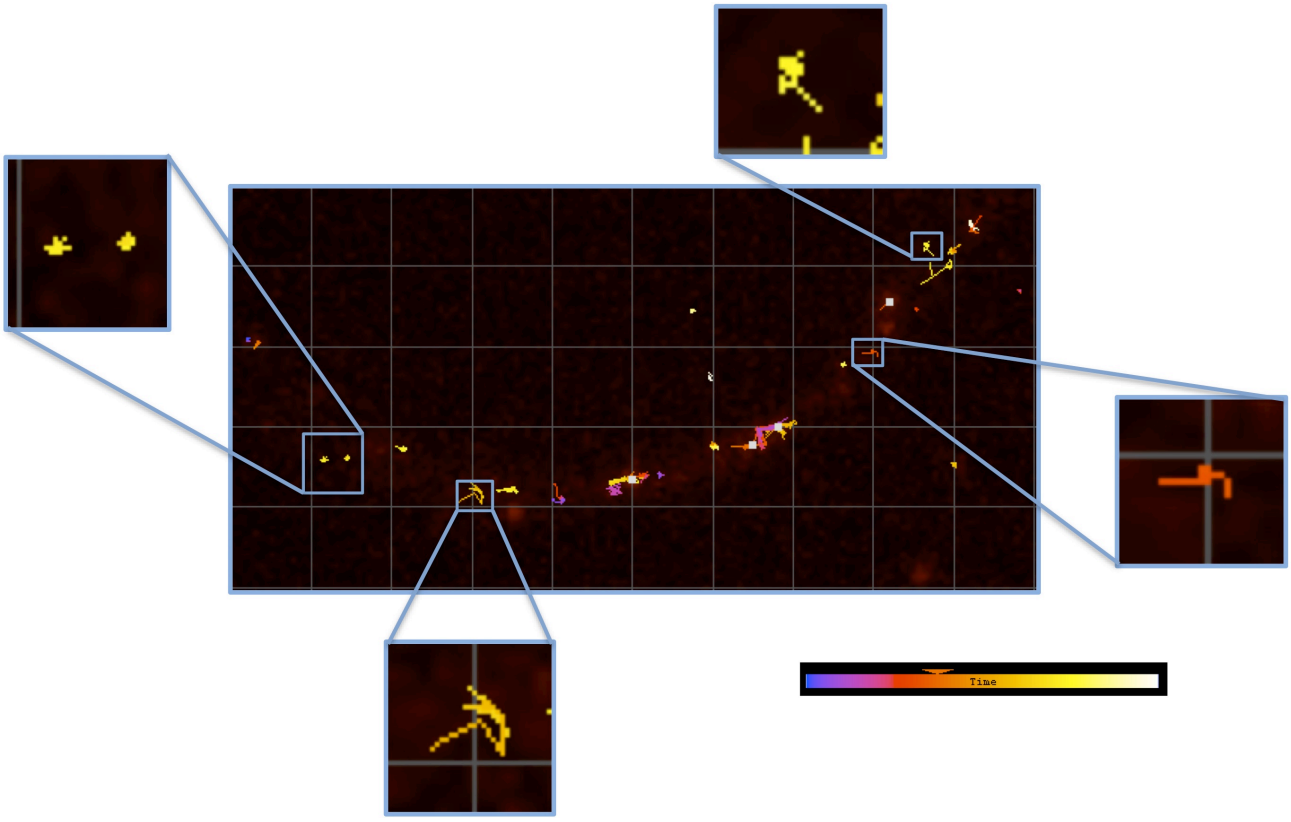

Figure 2-6. Cellobiohydrolase I Trajectories on Cellulose over one hour
Numerous labeled enzymes were tracked on *V. ventricosa* microcrystals with the time scale indicated by color. Motions in blue occur first during the incubation (t=0) and those in white occur last (t = 60 min). Some enzymes remain stationary during this time course, while others show a series of behaviors—stationary, linear, and 2-D Brownian motion—in various permutations.

Movement on Cellulose				
	Linear	Nonlinear	Stationary	Transient
Proportion of Total (%)	1.2	5	42.5	52.3
Average Rate (nm/s)	10.4	130.1	--	--

Table 2-1. Populations of CBH I motion observed on crystalline cellulose
Surprisingly, a large population of enzymes remain stationary for extended periods of time. Our bulk assay activities predict an average rate of 0.15nm/s.

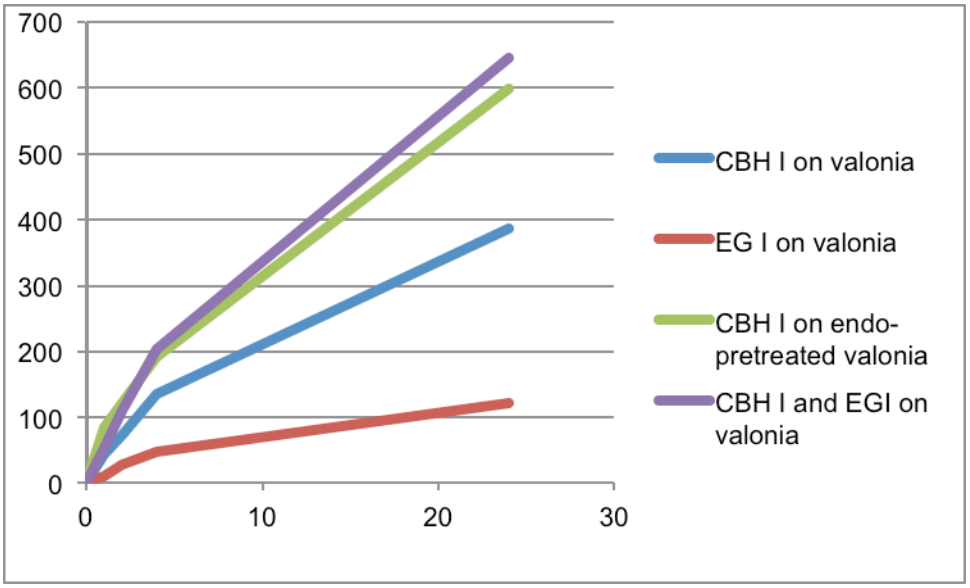

Figure 2-7. CBH I Activity on *Valonia ventricosa* Cellulose after Endoglucanase Pretreatment or during Concurrent Endoglucanase Incubation
Total soluble sugars released (uM) over 24 hours. Treatment of cellulose with an endoglucanase creates more operational sites for CBH I. With both pre- and concurrent treatment, CBH I shows greater activity than without any endoglucanase action. The synergism observed is expected to affect the distribution of CBH I movements and shift the enzymes to more productive states. The close activities of pretreated and concurrently treated EG I are hypothesized to be due to an excess of cellulose in this assay, which mimics microscopy conditions.

	Movement on Cellulose			
	Linear	Nonlinear	Stationary	Transient
Untreated Cellulose				
Proportion of Total (%)	1.2	5	42.5	52.3
Endo-Pretreated Cellulose				
Proportion of Total (%)	4.8	3.2	53.2	38.8

Table 2-2. Populations of CBH I motion observed on cellulose microcrystals and on endo-pretreated microcrystals.
After pretreating cellulose microcrystals with EG I, a higher percentage of CBH I enzymes are found to be linearly moving as well as stationary. Fewer are found to move nonlinearly or to quickly dissociate from the surface. Pretreatment of cellulose with an endoglucanase should shift enzymes to more productive states, since CBH I activity is higher on this substrate. As expected, more appear processive, but, surprsingly, more are also stationary, at least within these limits of resolution. Average rates could not be determined.

A. **B.**

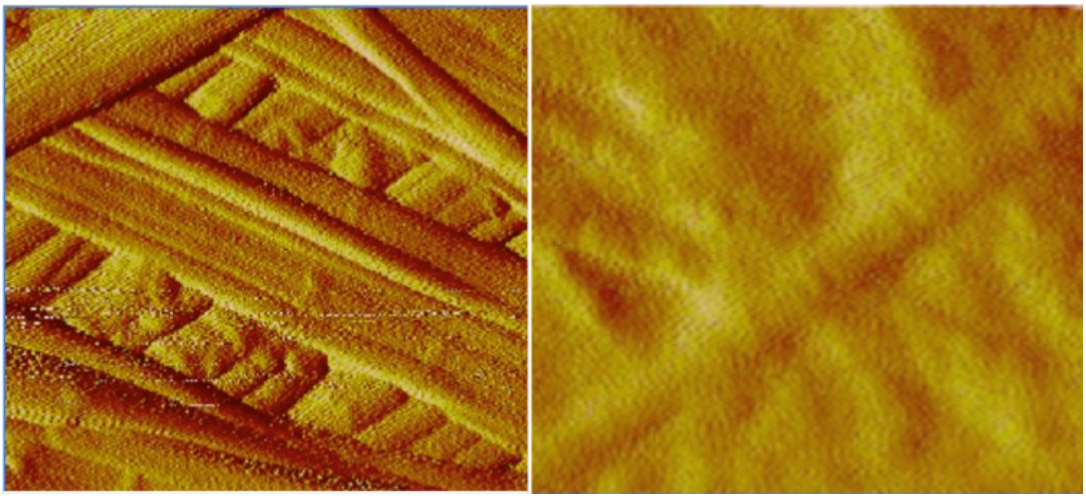

Figure 2-8. AFM imaging of *Valonia ventricosa* Cellulose before and after CBH I digestion
Valonia Ventricosa cellulose was incubated with *T. reesei* Cellobiohydrolase I for 24 hours. Representative before (A) and after (B) fluid tapping mode images are shown. Here, cellulose microfibrils are observed to form macrofibrils, and these bundles can be seen in a lattice formation in the algal cell wall. Treatment with CBH I disintegrates most of the cellulosic ultrastructure. Both images are 500 x 500 nm.

Surface Measure	Untreated	CBH I - treated
Width Range of Microfibrils (nm)	18.6 - 76.3	19.7 - 101.8
Mean Width of Microfibrils (nm)	33.6	48.2
Width Range of Macrofibrils (nm)	74.9 - 179.8	65.6 - 151
Mean Width of Macrofibrils (nm)	112.4	88.6
Mean Z range (nm)	85.2	49.1
RMS Roughness (nm)	38.9	21.7
Projected Surface Area Difference	32%	9%

Table 2-3. Summary of Surface Changes After Cellobiohydrolase I Treatment
Characterization of surface changes after CBH I treatment. Micro- and Macrofibrils are smoothed over during the course of hydrolysis; the height (Z) range, RMS roughness, and surface area all diminish. These findings indicate that over the course of hydrolysis with CBH I, the surface becomes more flat, and that surface features provide accessible binding sites for degradation.

A.

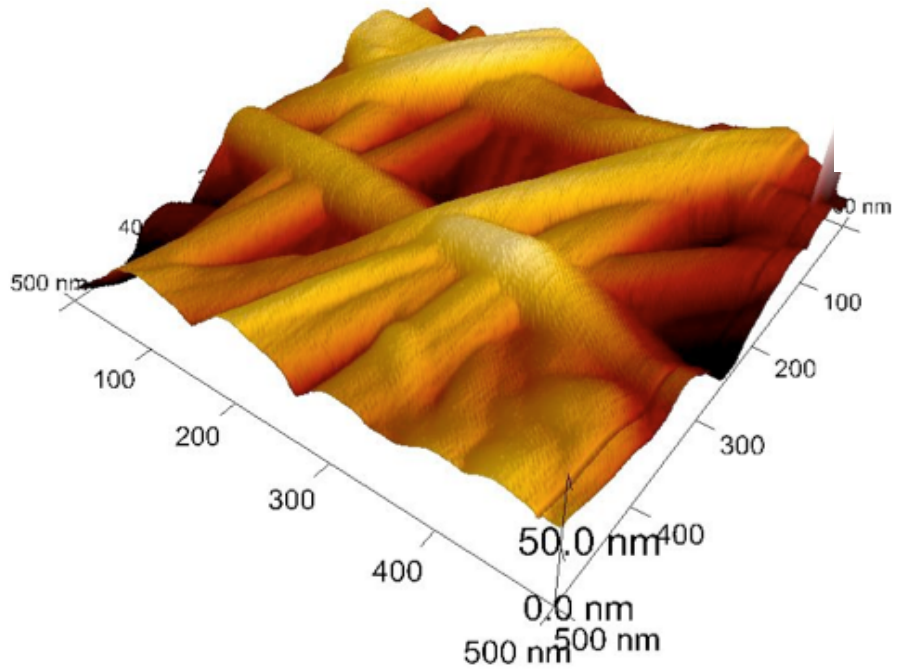

B.

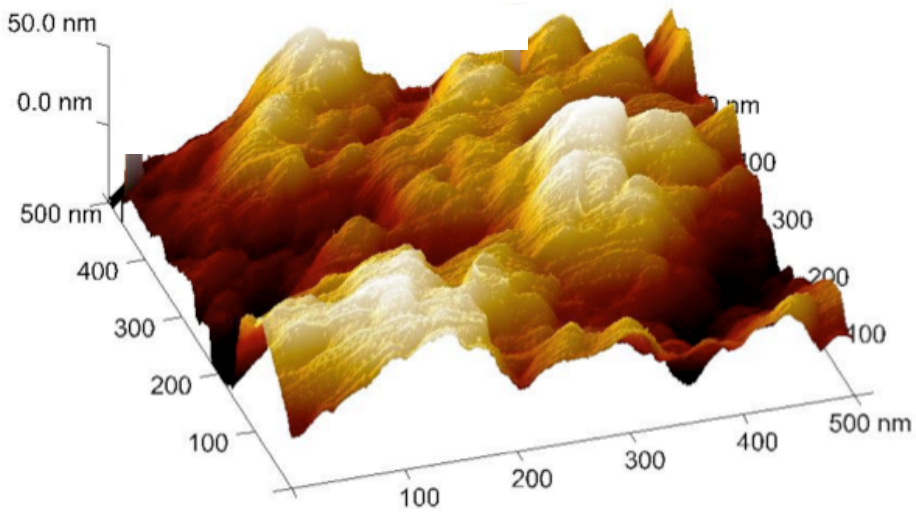

Figure 2-8. AFM Imaging of *Valonia ventricosa* Cellulose Before and After Treatment with Ionic Liquids

3-D rendering of tapping mode images. *Valonia ventricosa* cellulose is among the most crystalline known (A), but after treatment with ionic liquids it degenerates into amorphous forms (B).

A.

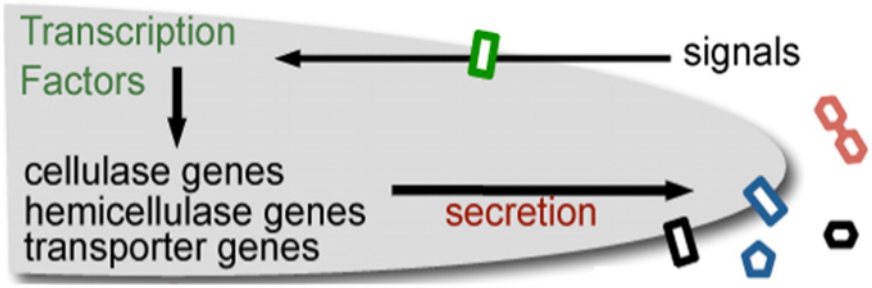

B.

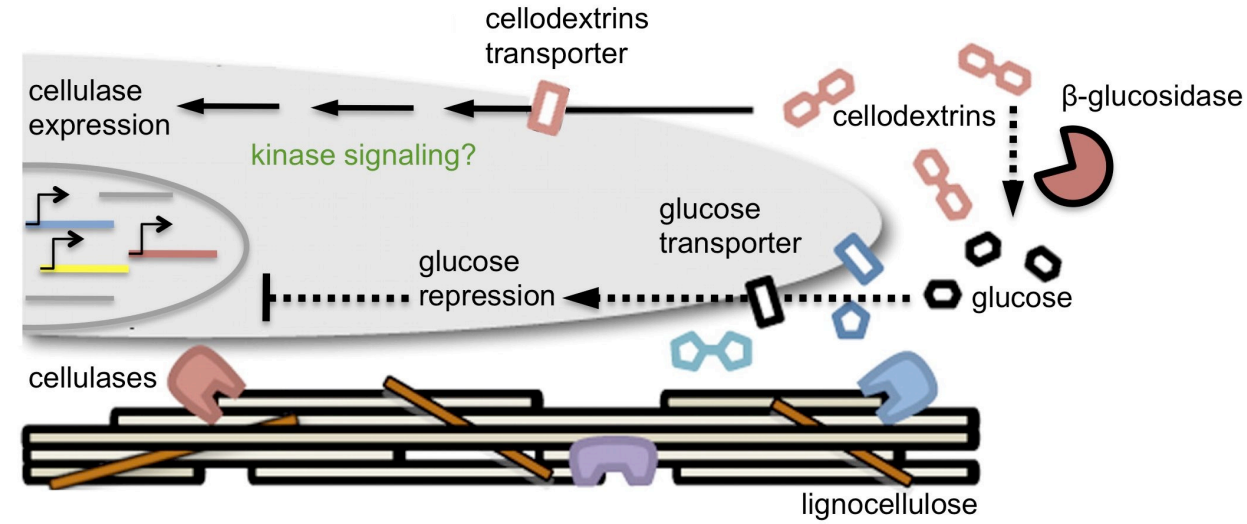

Figure 3-1. Model of Cellulase Upregulation in *N.crassa*.

A. In the previously proposed model (top) [48], a basal level of cellulase scavenger enzymes are secreted and generate an unknown signaling molecule that is transported into the cell. This signal leads to the significant upregulation of cellulase, hemicellulase, and transporter gene transcription and expression, and eventually the degradation and consumption of the cellulosic substrate.

B. In the refined model proposed here, cellodextrins enter the cell through their own transporters and signal through one or more kinases or signaling enzymes to activate transcription factor(s), which then induce cellulases and other enzymes for cellulose utilization.

FGSC	NCU	Functional Prediction (and yeast/human homologs)	Relative CMCase Activity to WT
11318	NCU06419	MAP Kinase Kinase (Sc-MKK1)	0
11546	NCU06563	S/T-Protein Phosphatase (Sc-PPG1/Hs-PP2A)	0.1
12547	NCU09123	Calcium/Calmodulin-Dependent Protein Kinase	0
15781	NCU06330	Phosphatase	0.5
17400	NCU00188	Kinase	0
17963	NCU07399	Kinase (Sc/Hs-Stk16)	0.1
19644	NCU08158	Phosphatase (Sc-YVH1)	0.4

Table 3-1. Summary of KOs Identified as Cellulase Activators.
Seven deletion strains found to have cellulose-specific growth defects. The corresponding supernatant endoglucanase (CMCase) activity is listed, as well as functional predictions and any known *Saccharomyces cerevisiae* (Sc) or human (Hs) homologs. ΔNCU07399/FGSC1793 exhibited the most severe phenotype on Avicel and was chosen for further study. Though several strains showed low supernatant activity, it is speculated their cellulases were engaged on the cellulose surface enabling avicel degradation. ΔNCU07399 depolymerized the least amount of cellulose of all strains observed, as visualized on Day 7 growth flasks (See Figure 3-2 for further detail).

A.

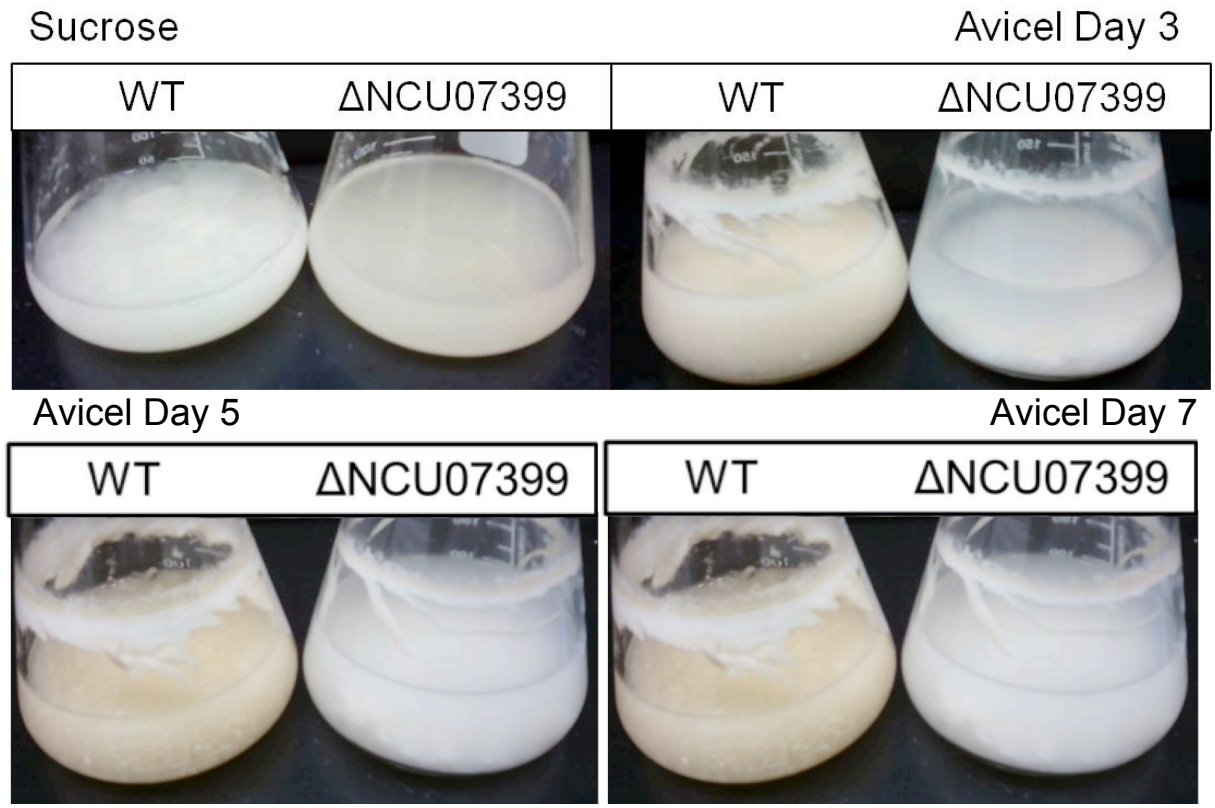
Sucrose
Avicel Day 3
WT
ΔNCU07399
WT
ΔNCU07399
Avicel Day 5
Avicel Day 7
WT
ΔNCU07399
WT
ΔNCU07399

B.

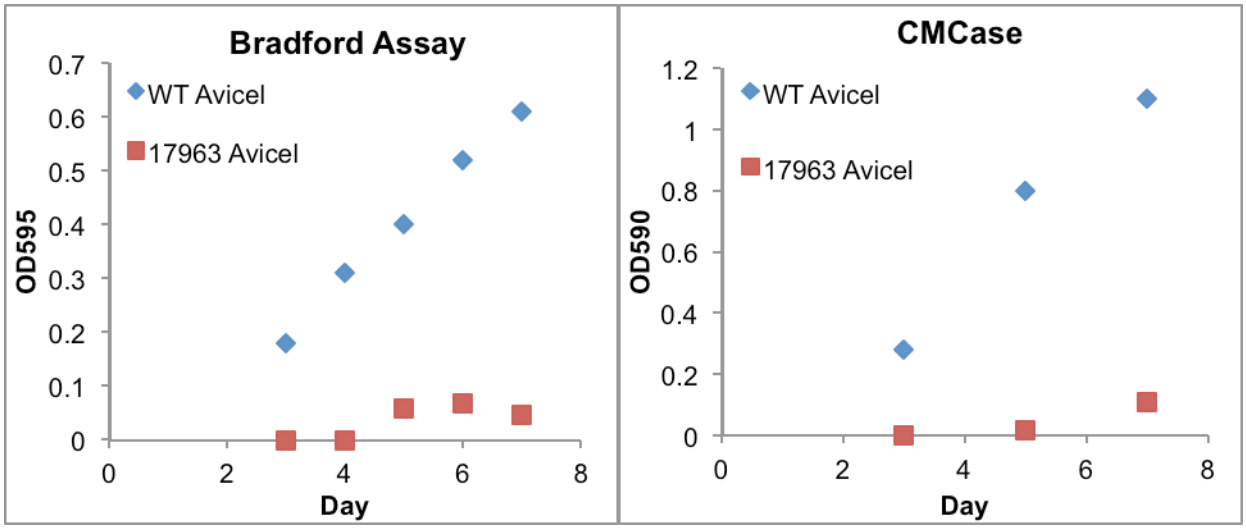
Bradford Assay
OD595
0.7
0.6
0.5
0.4
0.3
0.2
0.1
0
0
2
4
6
8
Day
WT Avicel
17963 Avicel
CMCase
OD590
1.2
1
0.8
0.6
0.4
0.2
0
0
2
4
6
8
Day
WT Avicel
17963 Avicel

Figure 3-2. Growth, Protein Secretion, and Endoglucanase Activity of WT and ΔNCU07399 on Sucrose or Cellulose Media.

A. WT and ΔNCU07399 grown on Vogel's sucrose or Vogel's avicel media. After 48 hours, the deletion strain culture appeared nearly identical to the WT strain, showing only a slight difference in coloration. On cellulose, ΔNCU07399 showed a clear growth defect and was unable to degrade avicel in the media. In the WT culture, mycelia filled the flask and after seven days the avicel was nearly fully consumed. In the deletion strain, only a small fungal mat was observed and very little cellulose was degraded.
B. Supernatant samples were removed from the Avicel cultures after 3, 5, and 7 days of growth. Bradford and CMCase assays were used to monitor cellulases in the supernatant. A steady rise in supernatant protein concentration and endoglucanase activity was seen for WT, but only barely observed after 5-7 days of growth for ΔNCU07399.

A.

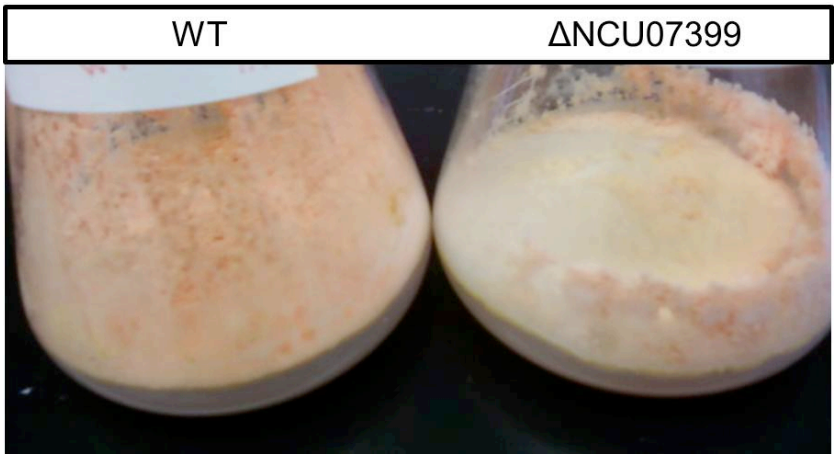

B.

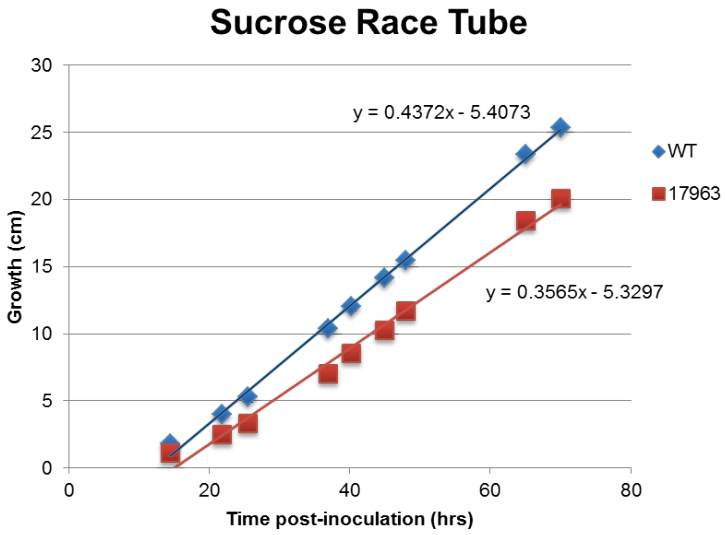

Figure 3-4. WT and ΔNCU07399 Growth on solid sucrose media.

A. Wild type *N. crassa* grown on Vogel's sucrose-agar media (left) showed dense, fluffy growth and an extension of aerial hyphae, as well as abundant conidiation (spore formation). By contrast, ΔNCU07399 grown on solid sucrose media (right) displayed stunted growth of aerial hyphae and low conidiation levels.

B. WT and ΔNCU07399 were grown on Vogel's sucrose-agar race tubes and mycelial growth was measured over 3 days to determine the rate of fungal extension. ΔNCU07399 grew at approximately 80% the rate of WT, and thus the sucrose growth defect was not considered significant.

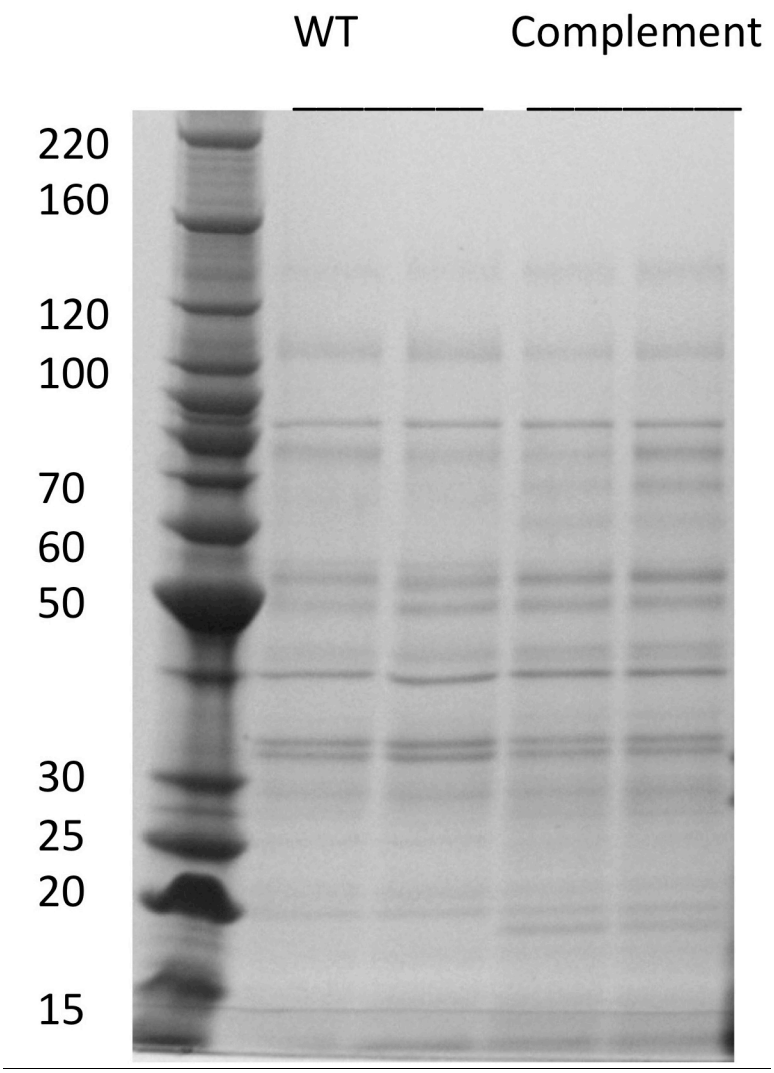

Figure 3-5. Secretion Profile of WT and ΔNCU07399 Complementation. ΔNCU07399 was mated to an *N. crassa* strain with an additional copy of NCU07399 in its *his3* locus. Ascospores were selected that contained the deletion of NCU07399 in the native locus (hygromycin resistance). Four out of ten showed wild type-like growth on sucrose slants as well as in sucrose and avicel liquid cultures (data not shown). The wild type-like strains were then genotyped to confirm the hygromycin resistance cassette. In these NCU07399 complement strains, all sexual and vegetative defects were restored by the presence of NCU07399 in the *his3* locus. Here, an SDS gel of the proteins secreted by WT and the ΔNCU07399 complement when grown on avicel is shown. Lane 1, molecular weight markers in kDa; lanes 2-3, WT secretome; lanes 4-5, complement secretome. The samples were taken from biological duplicates and unconcentrated supernatant was loaded in each lane.

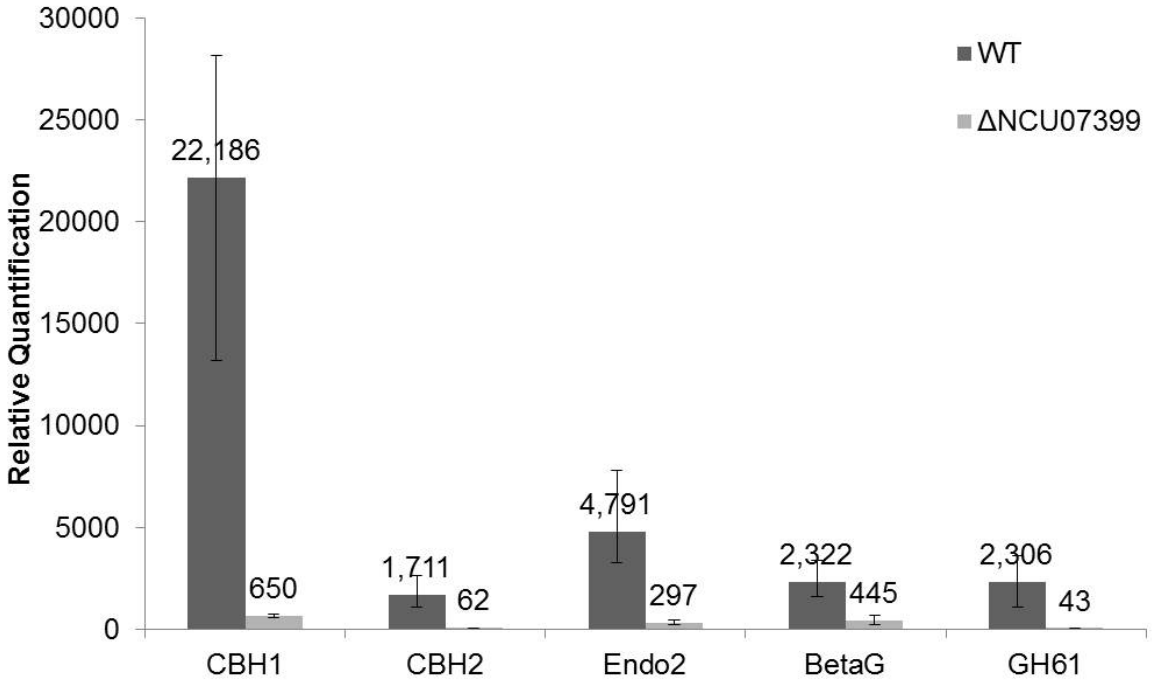

Figure 3-6. Induction of Cellulases in WT and ΔNCU07399 in Response to Cellulose.

Cellulase upregulation after incubation with avicel or sucrose for four hours. The three major cellulases, Cellobiohydrolase I (CBH I), Cellobiohydrolase II (CBH II) and Endoglucanase II (EG II), as well as β-glucosidase (BetaG) and Glycoside Hydrolase 61 (GH 61) were analyzed by qPCR. Transcripts from the WT culture are in dark grey and those from ΔNCU07399 are in light grey. Experiments were carried out in biological triplicate, with the standard deviation from the mean shown.

A.

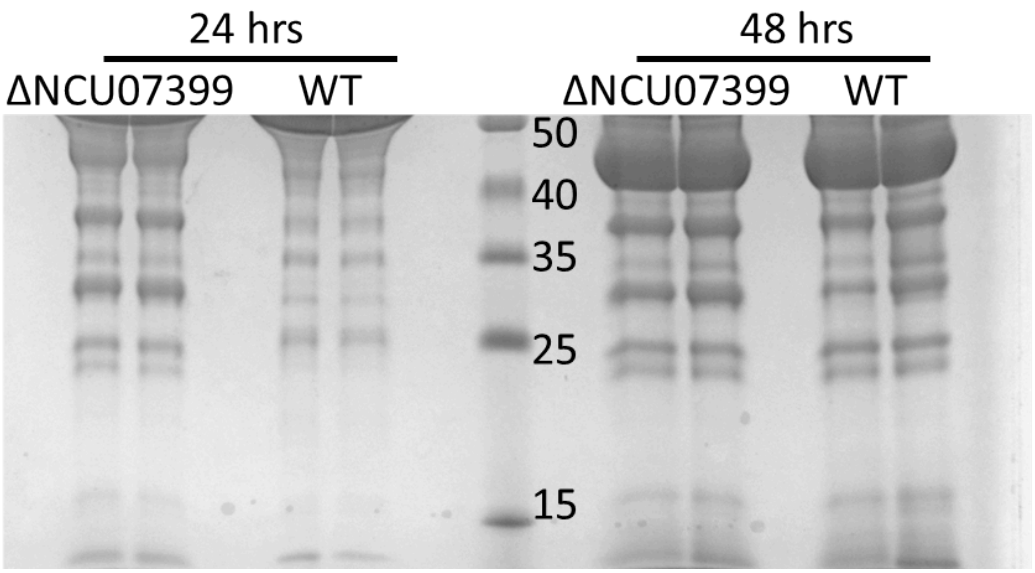

B.

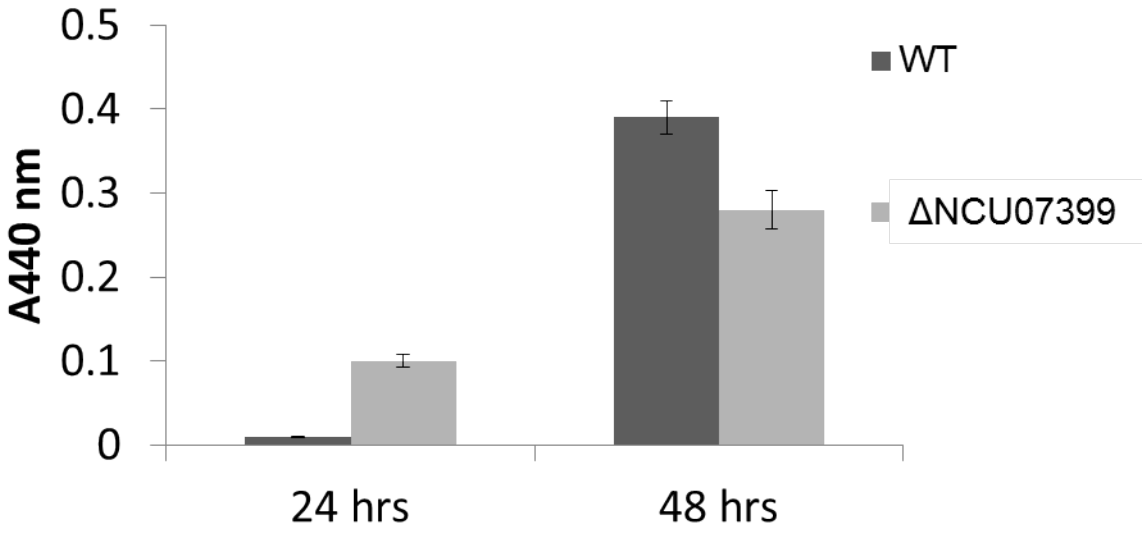

Figure 3-7. WT and ΔNCU07399 Protease Secretion and Activity on BSA Media

A. ΔNCU07399 and WT were grown on BSA media to test for secretion defects. Samples taken at 24 and 48 hours were analyzed by SDS-PAGE. Culture supernatants from biological duplicates are shown, along with a molecular weight marker (kDa).

B. Filtered culture supernatants were used in an azo-casein protease assay to monitor nonspecific proteolytic activity from ΔNCU07399 and WT strains at 24 and 48 hours.

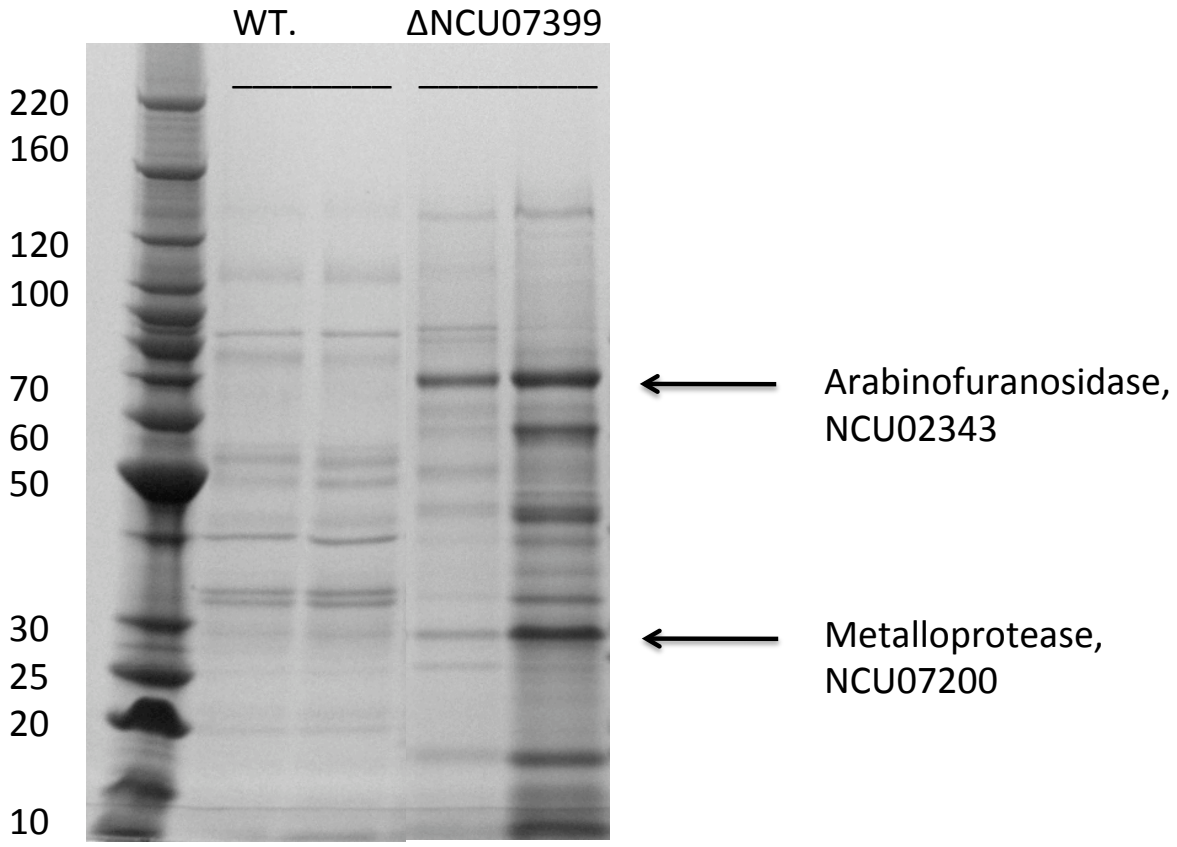

Figure 3-8. Secretion Profile of WT and ΔNCU07399.
WT and ΔNCU07399 supernatants collected after seven days of growth on avicel. The KO samples were concentrated 20-50 fold. Lane 1, molecular weight markers in kDa; lanes 2-3, supernatant from duplicate WT cultures; lanes 4-5, supernatant from duplicate ΔNCU07399 cultures. Several previously identified proteins were confirmed, however, two new supernatant enzymes were found highly induced in the KO strain supernatant. They include an arabinofuranosidase (NCU02343) as well as a metalloprotease (NCU07200). The presence of this metalloprotease in part explains why so little protein is found in the deletion strain culture supernatant.

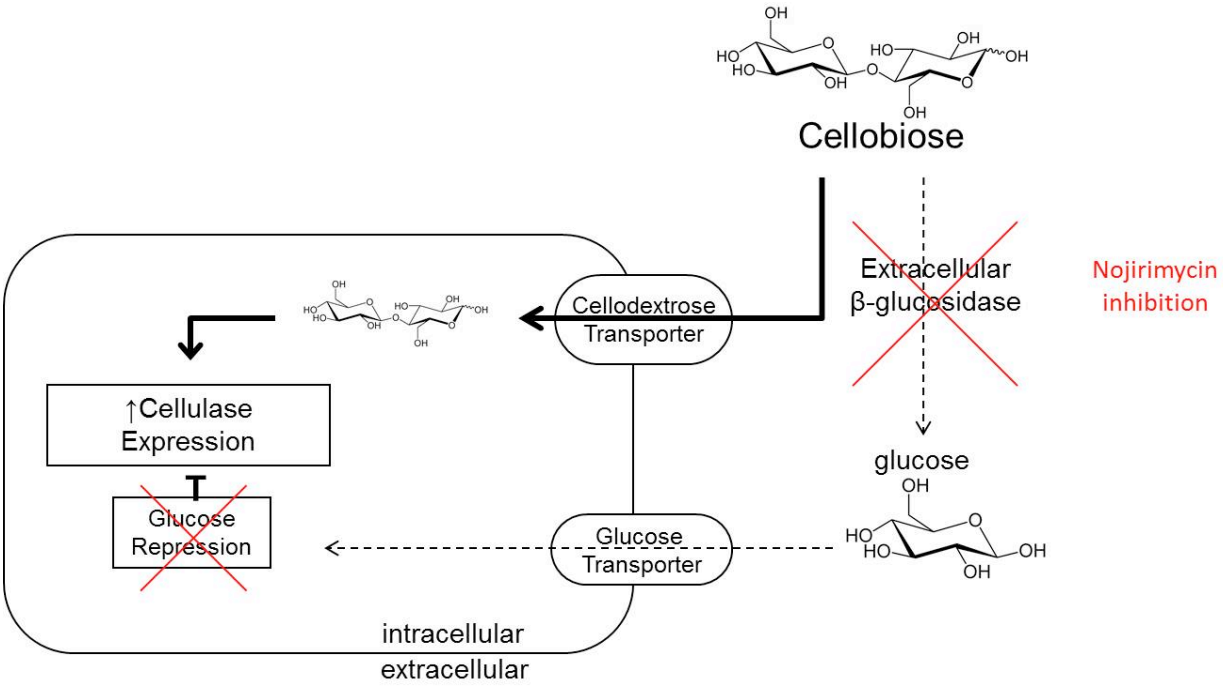

Figure 3-9. Addition of nojirimycin partially relieves glucose repression and allows cellobiose to act as an inducer in *N. crassa*.
During growth on cellobiose, extracellular β-glucosidases are thought to cleave cellobiose into two glucose units which enter the cell through a glucose transporter and lead to glucose repression of cellulase genes [42]. The effects of nojirimycin addition on the system are seen in red. Nojirimycin inhibits extracellular β-glucosidases when added to the media, which allows cellobiose to enter cells through the cellodextrin transporter and signal a partial cellulase induction.

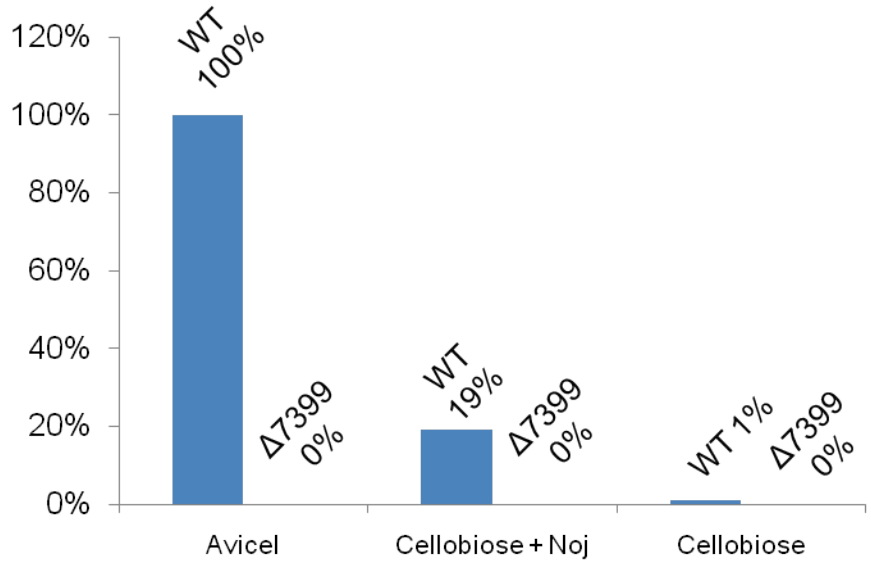

Figure 3-10. WT and ΔNCU07399 MULac activity after transfer to Avicel, cellobiose, or cellobiose + nojirimycin
MULac activity is all shown relative to WT *N. crassa* grown on Avicel, where the most cellulase activity is observed. During growth on cellobiose alone, neither WT or ΔNCU07399 produce cellulases with MULac activity due to the glucose repression provided by the β-glucosidase cleavage of cellobiose [42]. When the β-glucosidase is inhibited with nojirimycin, WT cultures had 19% of the MULac activity found in Avicel samples. No activity was detected in any of the ΔNCU07399 samples, indicating that the relief of glucose repression does not allow for cellulase induction by the strain.

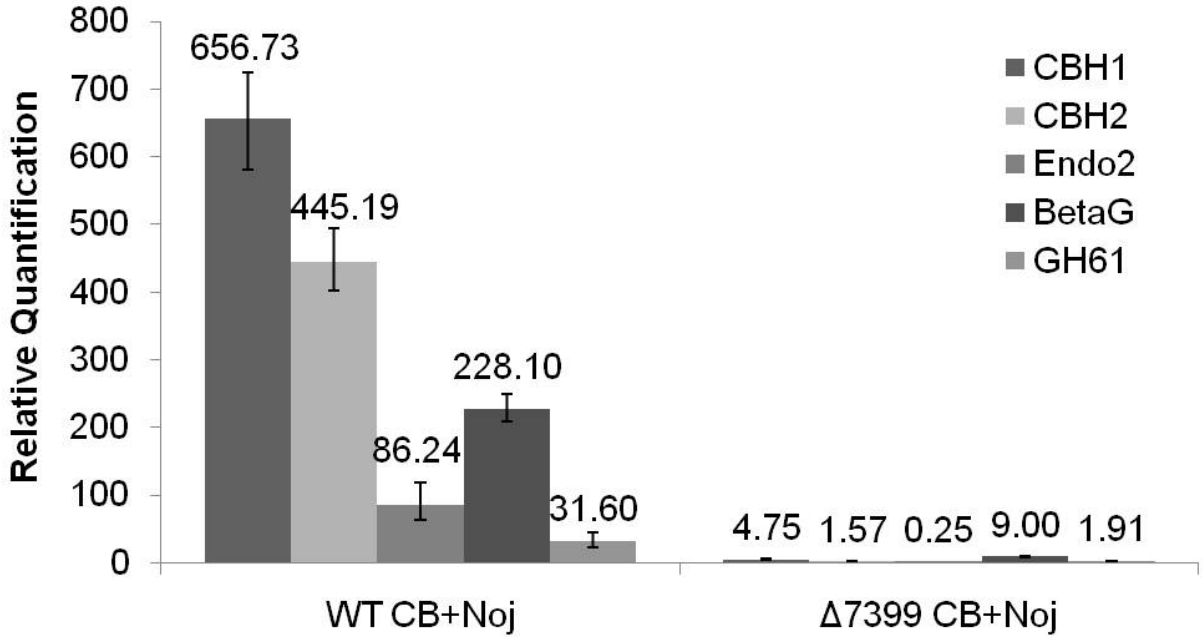

Figure 3-11. qPCR of WT and ΔNCU07399 *N. crassa* mRNA after growth on cellobiose + nojirimycin

Total RNA extracted from cultures grown on cellobiose + nojirimycin for 4 hours (see Materials and Methods) was used to measure the relative level of mRNA transcripts for five major secreted proteins in comparison to cellobiose grown cultures. The five proteins are the same as in Figure 3-6. The level of transcripts detected in WT samples did not parallel the induction seen on Avicel, but all genes tested were induced. ΔNCU07399 showed little to no increase in transcripts, except for an intracellular β-glucosidase (RQ = 9). Each experiment represents a biological triplicate, with the standard deviation shown.

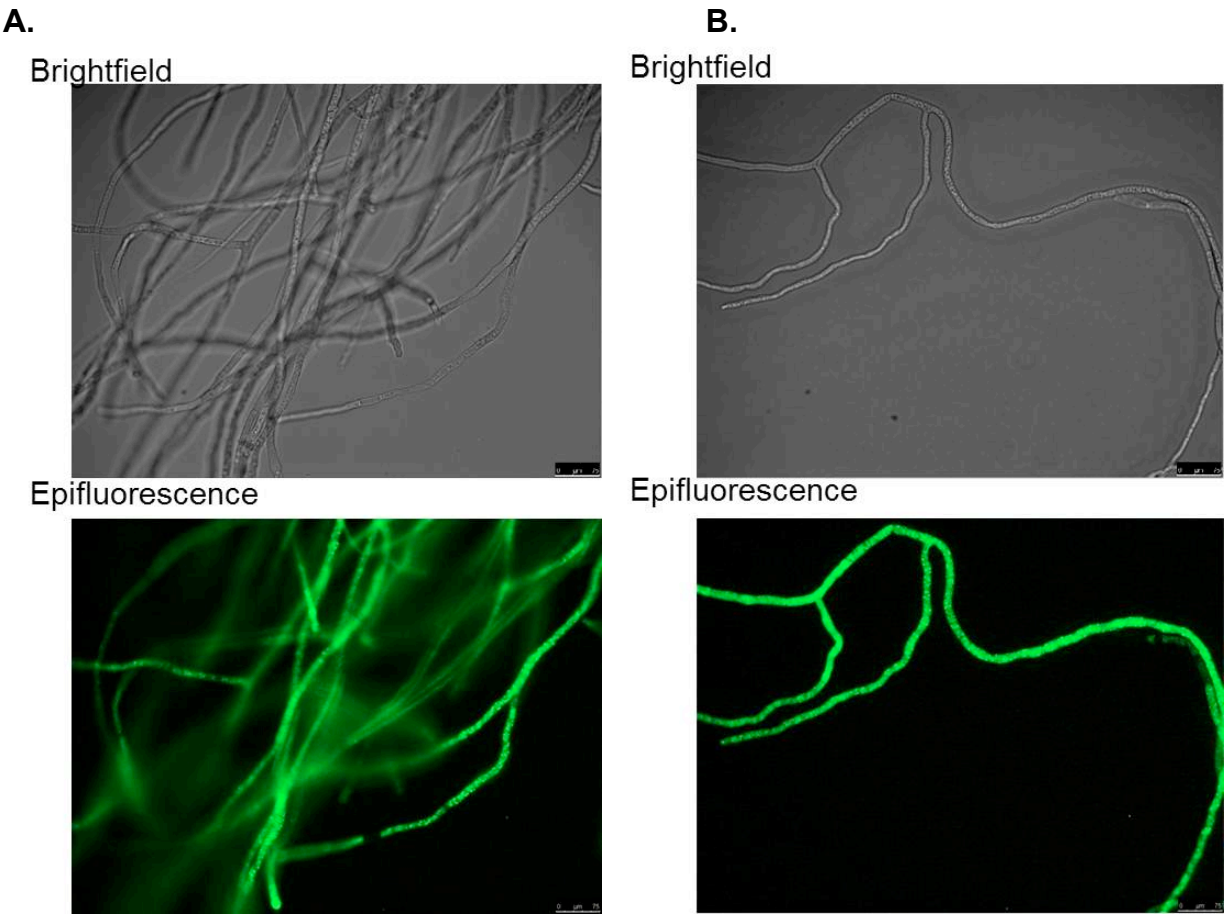

Figure 3-12. Fluorescence of NCU07399-GFP expressed in WT *N. crassa.* Constructs containing NCU07399 with a C-terminal GFP tag were transformed into WT *N. crassa* and visualized by microscopy. The brightfield images are shown above with the epifluorescence images of the visualized GFP tagged proteins below. Two constructs were prepared, the standard NCU07399 (A) and a mutant with the catalytic aspartate 238 changed to alanine, NCU07399-KD (B).

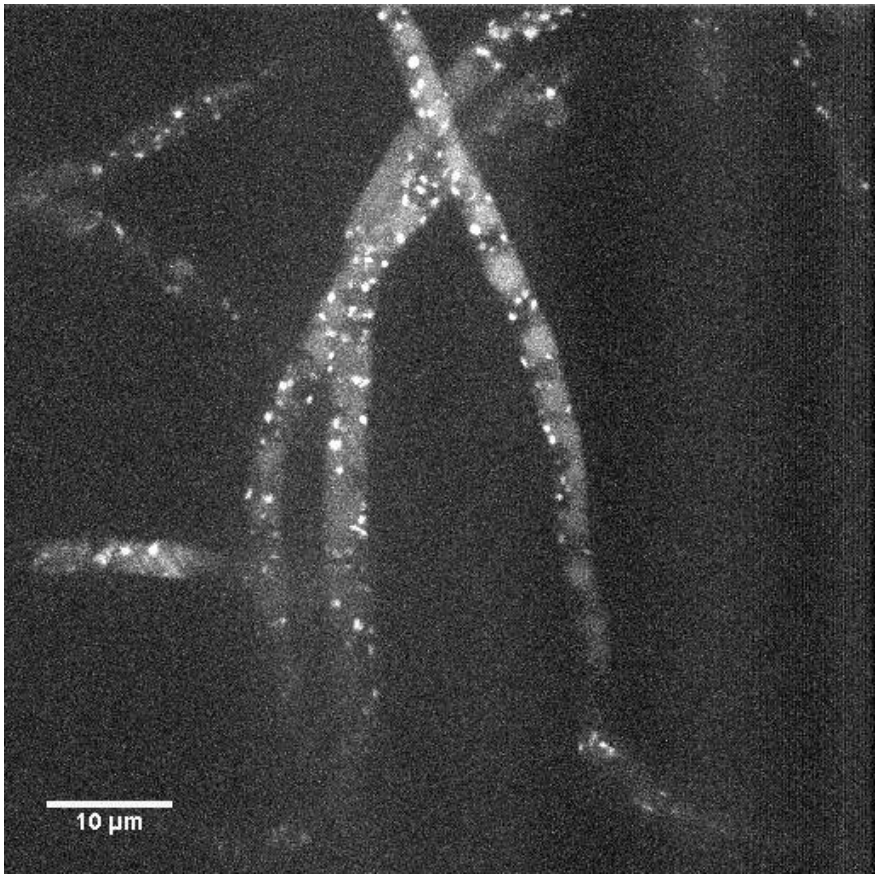

Figure 3-13. NCU07399-GFP localization in WT *N. crassa* mycelia
A construct containing NCU07399 with a C-terminal GFP tag was transformed into WT *N. crassa* and visualized by confocal microscopy. The distribution of the kinase appears to be both diffuse in the cytoplasm as well as localized in punctuate spots, but does not collect in the nucleus. Images were similar for both the NCU07399-GFP strain and the catalytically dead NCU0739-KD-GFP strain.

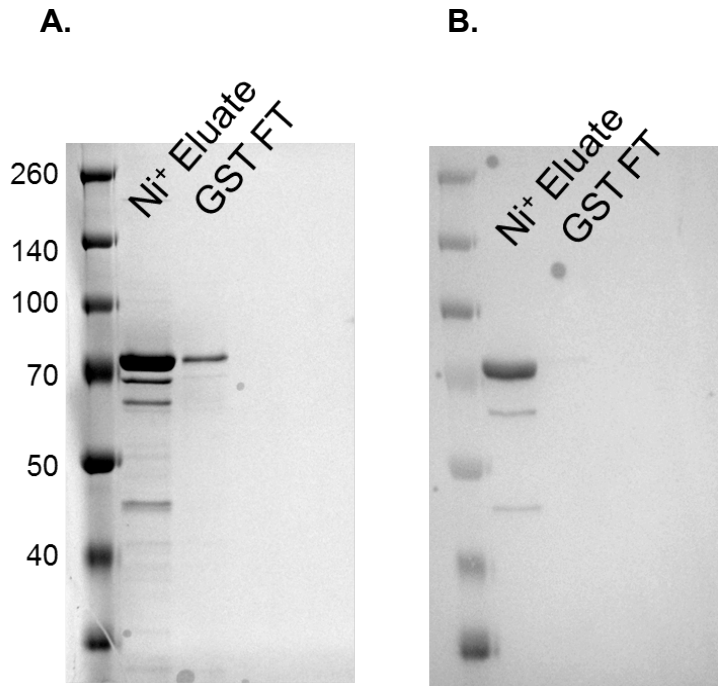

Figure 3-14. Expression and purification of NCU07399 in *E. coli*.

A. The *E. coli* lysate of cells expressing NCU07399 were run over an Ni-NTA column and the eluate from the column was used in a second purification using the GST tag. The Ni-NTA eluate was mostly pure and the GST tag did not seem to stick to the second column. The semi-purified Ni-NTA eluate was used for all subsequent reactions. Lane 1, molecular weight marker in kDa; lane 2, Ni-NTA eluate; lane 3, flow-through from the glutathione resin.

B. A Western blot using an anti-6xHis antibody of the same gel showed the His-tagged kinase to be the major band in the purification and that several smaller degradation products could be detected.

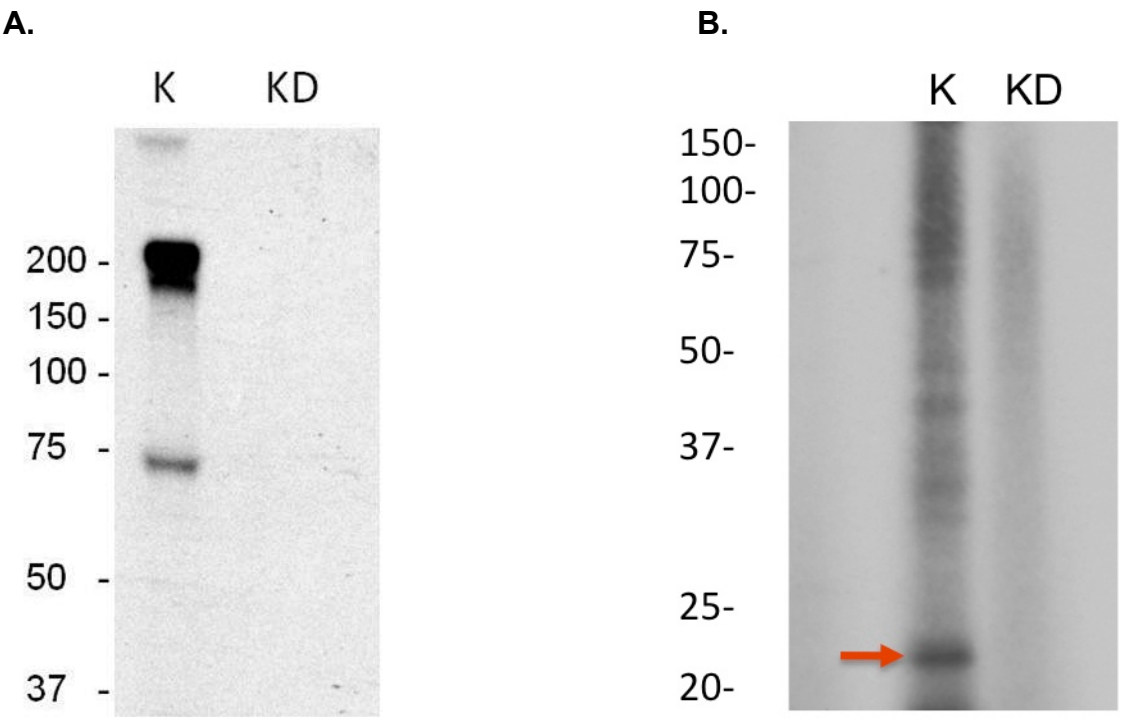

Figure 3-15. NCU07399 *in vitro* Phosphorylation.
E. coli purified NCU07399 was tested *in vitro* for autophosphorylation (A) and the transphosphorylation of myelin basic protein (B), a model kinase substrate. Both reactions used γ-[^{32}P]-ATP and either the wildtype kinase (K) or the kinase dead catalytic mutant (KD). The transphosphorylation assays also included MBP. In either case, the KD mutant did not display any activity, confirming that the correct catalytic residue was identified for the kinase. The autophosphorylation radiogram shows the activated enzyme at ~72kD as well as phosphorylated high molecular weight band(s). These have been identified by mass spectrometry to contain NCU07399, possibly as multimers. In the transphosphorylation assay, phosphorylated MBP is indicated with a red arrow. Thus NCU07399 is capable of both auto- and transphosphorylation, confirming its kinase activity. Samples were not heat-denatured before loading on the SDS gel. Molecular weights are shown to the left in kDa.

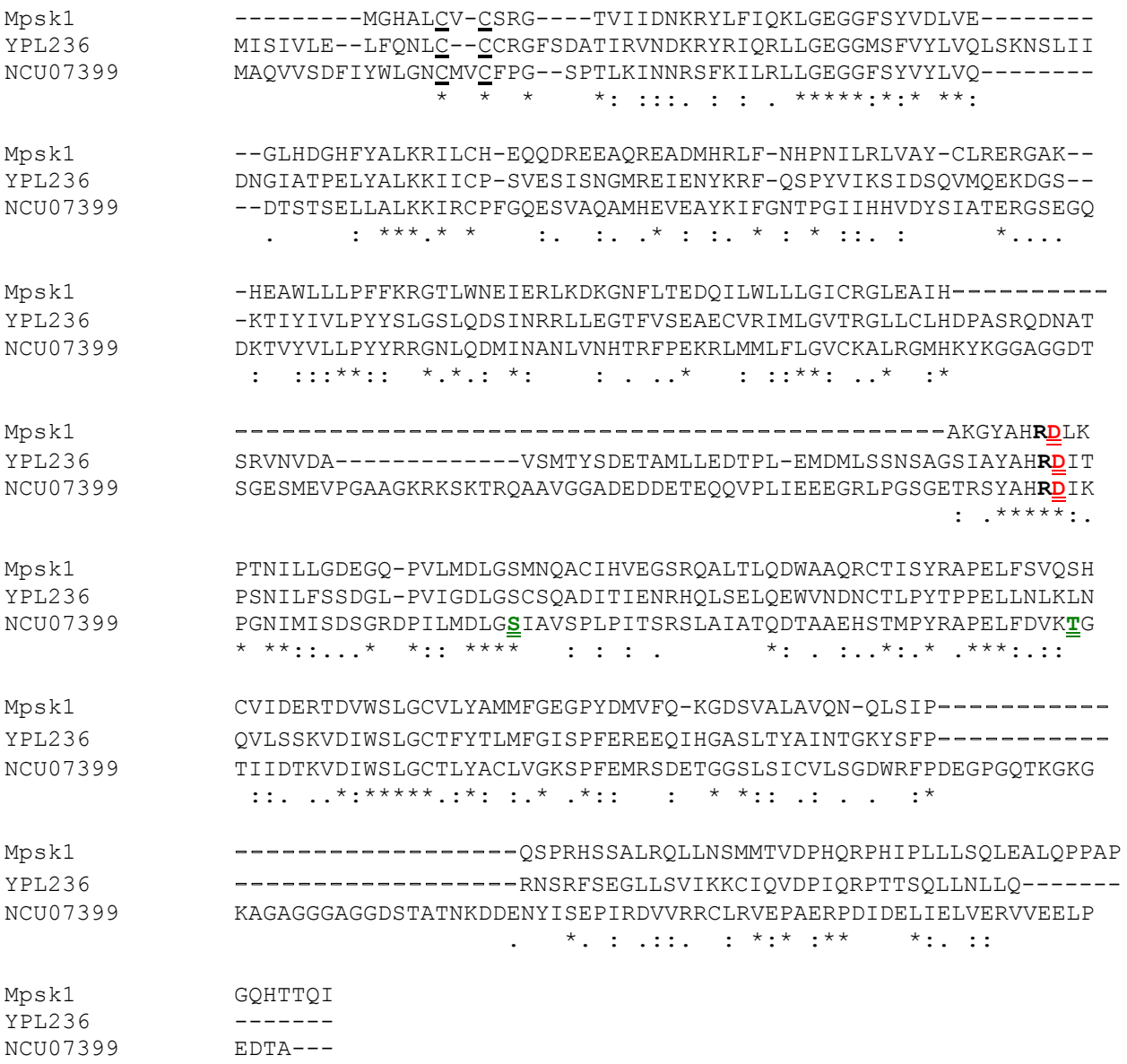

Figure 3-16. Alignment of NCU07399 with YPL236 and MPSK1.
The human (MPSK1) and yeast (YPL236) STK16 kinase sequences were aligned to NCU07399 using ClustalW, revealing several significant features. There are two insertions in the NCU07399 sequence resulting in an additional 110 amino acids. The confirmed catalytic aspartate is shown in red. The activation loop (shaded gray) has a conserved DLG—APE motif and with 37 residues is larger than in most studied kinases. Residues shown in green indicate identified phosphorylation sites. The phosphorylation of the earlier serine suggests NCU07399 might be activated by another upstream kinase, such as those in the MAP kinase pathway.

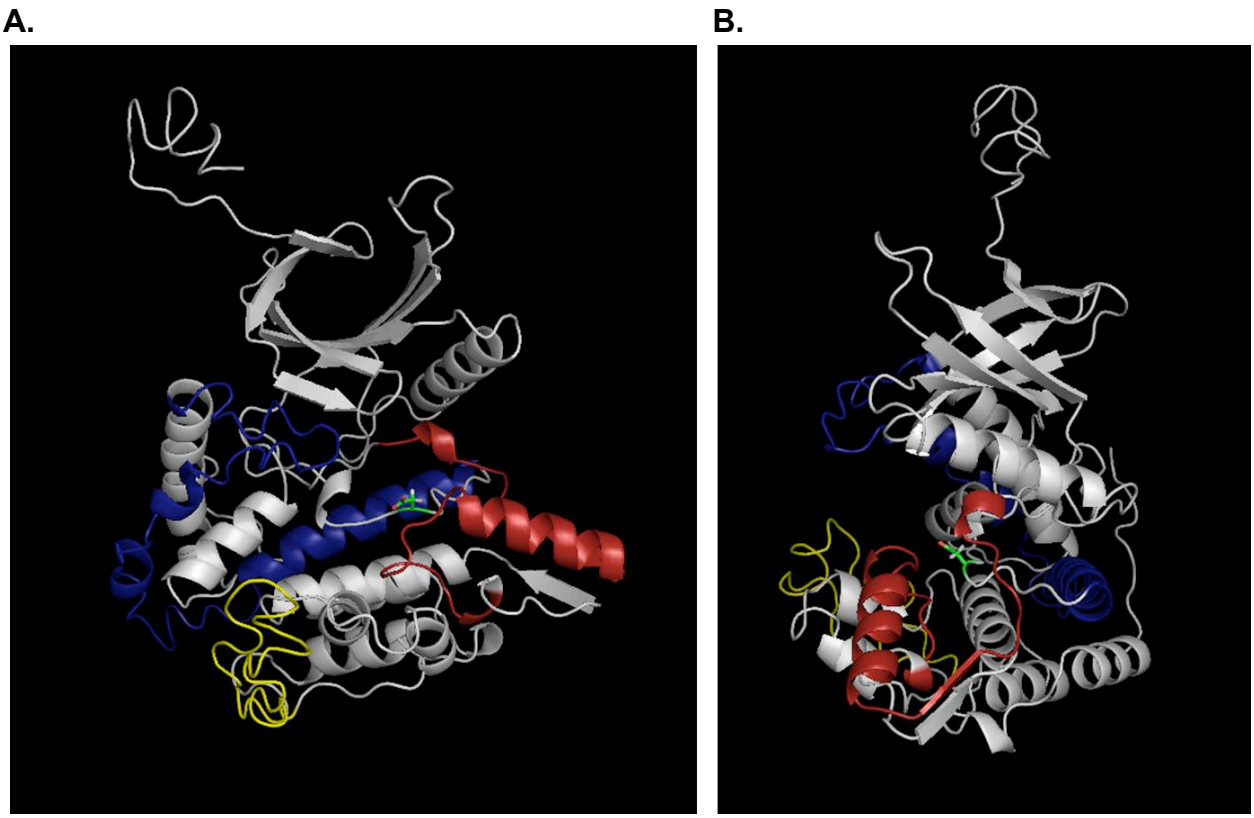

Figure 3-17. Homology model of the structure of NCU07399
Two views of the NCU07399 homology model, based on the structure of MPSK1 [84] are shown. The catalytic aspartate is shown in green. The atypical helical activaton loop is shown in red and the location of the two predicted insertions are in blue and yellow. The first insertion is predicted to have high helical content, while the second was fit as a random coil.

	CA	SC	CG	NC	PA	FG	HS
CA (*Candida albicans)*	100	42	43	38	41	41	38
SC (Saccharomyces YPL236**)	42	100	41	35	36	34	35
CG (*Chaetomium globosum*)	43	41	100	82	81	76	31
NC (*N. crassa* NCU07399)	**38**	**35**	**82**	**100**	**76**	**65**	**34**
PA (*Podospera anserina*)	41	36	81	76	100	64	34
FG (*Fusarium graminerium*)	41	34	76	65	65	100	36
HS (Human MPSK1)	38	35	31	34	34	36	100

Table 3-2 . Sequence identity matrix of *N. crassa* NCU07399 with several eukaryotic homologs.
A BLAST search revealed homologs of NCU07399 across a wide array of fungi, both cellulolytic and non-cellulolytic. The percent sequence identity of the human gene (MPSK1) and 5 fungal homologs is shown.

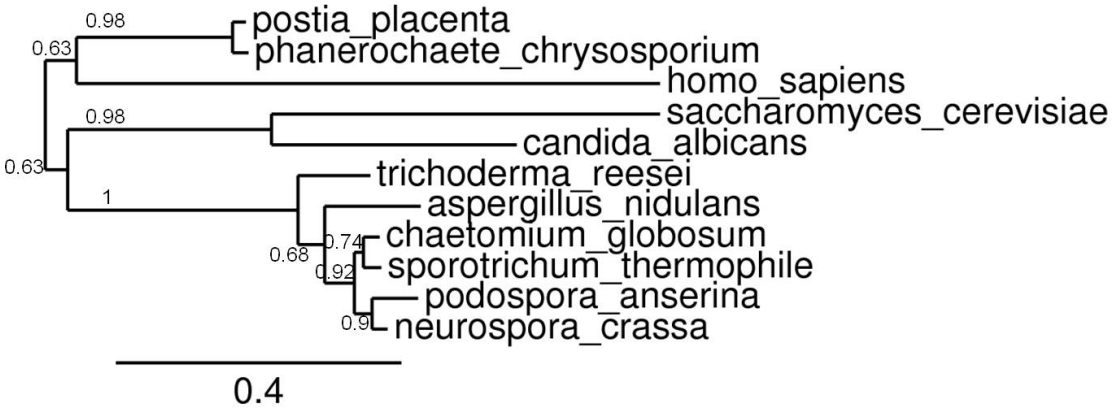

Figure 3-18. Phylogenetic Tree of NCU07399 with Orthologs from Select Organisms

NCU07399 and its ortholog counterparts in other organism are shown here. NCU07399, though it controls cellulase expression, has relatives in non-celluloylytic organisms including yeast. It clusters most closely with other ascomycetes, and further away from basidiomycetes *P. placenta* and *P. chrysosporium,* brown rot and white rot fungi, respectively.